STRUCTURE AND INFRASTRUCTURE ENGINEERING
2020, VOL. 16, NO. 2, 266–286
https://doi.org/10.1080/15732479.2019.1653937

Lifetime seismic resilience of aging bridges and road networks

Luca Capacci, Fabio Biondini and Andrea Titi

Department of Civil and Environmental Engineering, Politecnico di Milano, Milan, Italy

ABSTRACT

The performance of lifelines under damage and emergency conditions induced by sudden extreme events, such as earthquakes, can be assessed based on the concept of resilience. Damage also arises in time due to aging, affecting the structural performance of each network component and, consequently, impairing the overall system functionality. Furthermore, the sparse location over the network of vulnerable deteriorating structures, such as spatially distributed bridges, should be taken into account to establish proper infrastructure management policies. In this article, a probabilistic approach is proposed to assess the seismic performance of transportation networks considering the uncertainties involved in the lifetime structural response of aging bridges under different earthquake scenarios. The time-variant seismic capacity associated with prescribed limit states is evaluated by nonlinear incremental dynamic analysis. The initial damage induced by seismic events and its recovery process through structural repair is related to traffic restrictions to different road users. Traffic flow distribution analyses are carried out over the road network to assess the post-event system functionality and the corresponding seismic resilience. The role of different factors such as aging, earthquake scenario, and seismic capacity correlation is investigated by considering spatially distributed reinforced concrete bridges exposed to corrosion and highway networks with detours and re-entry links.

ARTICLE HISTORY
Received 18 September 2018
Revised 9 March 2019
Accepted 4 May 2019

KEYWORDS
Resilience; functionality; infrastructures; bridges; damage; aging; corrosion; life-cycle

Introduction

Planning proper lifeline management policies is a key task to satisfy the primary needs of communities not only under operational conditions, but also in a state of emergency. Resilience is becoming a driving concept for new generations of Building Codes and Standards, particularly in United States and Europe, informing innovative trends and practical policies for design, assessment, monitoring, and maintenance of strategic structures and infrastructure facilities. Several definitions of resilience can be found in literature, based on the epistemological orientation and theoretical background of the reference discipline (Gilbert, 2010). In civil engineering, resilience can be defined as the capability of the system to withstand the effects of extreme events and to recover promptly and efficiently the pre-event performance and functionality (Bruneau et al., 2003). Resilience of structure and infrastructure systems is generally investigated considering damage and disruptions caused by sudden extreme hazards, such as earthquakes (Biondini, Capacci, & Titi, 2015b; Bocchini & Frangopol, 2011, 2012a, 2012b; Bruneau & Reinhorn, 2007; Bruneau et al., 2003; Burton, Deierlein, Lallemant, & Lin, 2015; Capacci, 2015; Chang & Shinozuka, 2004; Cimellaro, Reinhorn, & Bruneau, 2010a, 2010b; Decò, Bocchini, & Frangopol, 2013; Franchin & Cavalieri, 2015). In this context, road infrastructure networks play an important role in the emergency response to seismic events and related hazards to ensure both a quick deployment of aids and resources to distressed communities and a prompt repair of the surrounding lifelines and buildings (Carturan, Pellegrino, Rossi, Gastaldi, & Modena, 2013; Zanini, Faleschini, & Pellegrino, 2017).

Consistently with graph theory, road networks are defined as a set of nodes and edges, i.e., vertices and arcs, respectively. Vertices can be referred to as specific points of interest used to define trip origins and destinations in the transportation system, while edges represent road segments and bridges in series that connect specific pairs of nodes (Thomson & Richardson, 1995). Among these elements, bridges are frequently the most vulnerable components (Basöz & Kiremidjian, 1998; Iwasaki et al., 1995; Yashinsky, 1995). The assessment of the residual structural capacity and the definition of ex-ante preventive retrofit interventions and ex-post effective recovery processes of bridges are hence key factors to ensure suitable resilience levels of road infrastructure networks (Billah & Alam, 2015). In particular, highway bridges are essential to guarantee suitable functionality levels and to prevent or minimise outages and disruptions in the aftermath of an earthquake (Bocchini & Frangopol, 2011; Chang, 2009). Indeed, damage of bridges causes direct economic losses due to repair interventions, as well as indirect losses due to network downtime and traffic delay. It is therefore important to minimise consequences of extreme events by ensuring the disaster resilience of highway transportation systems (Venkittaraman & Banerjee, 2014).

Nevertheless, for structural systems exposed to an aggressive environment, damage can also arise continuously in

CONTACT Luca Capacci luca.capacci@polimi.it

time due to the effects of aging and structural deterioration (Biondini, Bontempi, Frangopol, & Malerba, 2004, 2006; Biondini, Camnasio, & Palermo, 2014; Biondini & Frangopol, 2016, 2018; Frangopol, 2011; Jia & Gardoni, 2018; Kumar & Gardoni, 2014; Sanchez-Silva, Klutke, & Rosowsky, 2011; Yang & Frangopol, 2019). Consequently, seismic resilience of deteriorating structures and infrastructure systems depends on the time of occurrence of the seismic event (Biondini, Camnasio, & Titi, 2015a; Biondini, Capacci, & Titi, 2017; Capacci, Biondini, & Titi, 2016; Titi & Biondini, 2013; Titi, Biondini, & Frangopol, 2015). Furthermore, the fulfilment of modern requirements associated with traffic flow capacity during the entire service life of transportation facilities should guide road management policies towards the compliance of old roads to new construction standards (Papageorgiou, Mouratidis, & Eliou, 2012). Therefore, system functionality and seismic resilience should be formulated as time-variant performance indicators under a life-cycle perspective to properly support the decision making process and the definition of robust and comprehensive strategies for critical infrastructure management. Finally, the spatial distribution over the transportation road network of vulnerable aging structures, such as bridges, should be taken into account within a proper road management policy to assess the effectiveness of infrastructure investments, including the upgrading of existing road networks by building new highway branches (Capacci & Biondini, 2018a).

This article presents a life-cycle probabilistic approach to seismic performance assessment of spatially distributed aging bridges under different earthquake scenarios and resilience analysis of highway networks with detours and re-entry links. The time-variant seismic fragilities of the deteriorating bridges in the network are assessed for several limit states, from damage limitation up to collapse, through nonlinear incremental dynamic analysis (IDA) and Monte Carlo simulation. The level of seismic damage, which depends on the time of occurrence of the seismic event, is related to vehicle restrictions and traffic limitations. A traffic flow distribution analysis is carried out over the entire road network to compute the system functionality and the corresponding seismic resilience under prescribed post-event recovery scenarios.

The proposed approach is applied to reinforced concrete (RC) bridges exposed to chloride-induced corrosion, considering highway networks with detour and re-entry link. In particular, different network configurations are considered in order to investigate different levels of seismic capacity correlation among bridges, as well as the impact of the seismic event in terms of earthquake magnitude, epicentre location and seismic area source. The purpose of the applications is to show the detrimental effects of aging and structural deterioration on the seismic performance of bridge structures and seismic resilience of road networks and emphasise the importance of the earthquake scenario in a multi-hazard life-cycle-oriented approach to seismic design of resilient structures and infrastructure systems.

Structural deterioration of RC bridges under corrosion

Chloride-induced corrosion is a critical issue for RC bridges (American Society of Civil Engineers [ASCE], 2017). The damage suffered in time by materials, concrete and steel, affects the structural response of single members and the overall structure under service loadings, accidental actions and extreme events, such as earthquakes. In this article, the time-variant seismic performance is evaluated at the system level based on a general methodology for life-cycle probabilistic assessment of RC structures in aggressive environment (Biondini et al., 2004, 2006, 2014). This approach accounts for both the diffusion process of aggressive agents, such as chlorides, and mechanical damage induced by diffusion, which involves corrosion of reinforcement and deterioration of concrete (Bertolini, Elsener, Pedeferri, & Polder, 2004). The different sources of uncertainty related to random variability of material and structural properties, environmental exposure, diffusion process, and earthquake excitation are taken into account based on a probabilistic modelling of the involved random variables (Biondini et al., 2006, 2014).

Diffusion process

The Fick's laws of diffusion can effectively describe the process associated with chloride ingress in concrete. The diffusion process of a single component in an isotropic, homogeneous and time-invariant medium, can be reduced to the following second order partial differential linear equation (Glicksman, 2000)

$$D\nabla^2 C = \frac{\partial C}{\partial t} \tag{1}$$

where D is the diffusivity coefficient of the medium, $C = C(\mathbf{z},t)$ is the concentration of the chemical component at point $\mathbf{z}$ and time t, $\nabla C = \mathbf{grad}\ C(\mathbf{z},t)$ and $\nabla^2 = \nabla\cdot\nabla$. The numerical solution of Fick's diffusion equation is achieved by means of cellular automata (Biondini et al., 2004, 2006; Titi & Biondini, 2016). The exposure scenario is associated with the chloride concentration $C_0(\mathbf{z}_0,t) = C_0$ prescribed on the points $\mathbf{z}_0$ of the external surface of the member cross-section.

Corrosion damage

The initiation of corrosion damage at time t_{cr} is triggered by the attainment of a critical threshold of chloride concentration C_{cr}. The corrosion rate depends on the spatial concentration $C = C(\mathbf{z},t)$ of the chemical substance. Based on available data for chloride attacks (Bertolini et al., 2004), the following relationship is assumed (Biondini et al., 2004)

$$\frac{\partial \delta_s}{\partial t} = q_s C(\mathbf{z}, t), t \geq t_{cr} \tag{2}$$

where q_s is a damage rate coefficient.

The main effect of corrosion in RC structures is the mass loss of the reinforcing steel bars. The percentage loss of steel resistant area of a corroded bar can be described by means

of a dimensionless damage index $\delta_s = \delta_s(t)$ which provides a direct measure of deterioration within the range [0,1]. In this way, the time-variant area of the corroded bar is expressed as a function of the damage index as follows (Biondini et al., 2004)

$$A(t) = [1-\delta_s(t)]A_0 \quad (3)$$

where A_0 is the area of the undamaged bar.

The corrosion process may also involve a remarkable reduction of steel ductility even for a limited amount of mass loss (Almusallam, 2001; Apostolopoulos & Papadakis, 2008). Moreover, the formation of oxidation products may lead to the development of longitudinal splitting cracks in the concrete surrounding the corroded bars and, consequently, to delamination and spalling of the concrete cover (Al-Harthy, Stewart, & Mullard, 2011; Cabrera, 1996; Guzmán, Gálvez, & Sancho, 2011; Vidal, Castel, & Francois, 2004; Zhang, Castel, & François, 2010). Based on experimental evidence, these damage effects depend on the amount of mass loss and can be effectively modelled by relating the ultimate steel strain ε_{su} of the corroding bars and the compression strength f_c of the surrounding concrete to the damage index δ_s. The formulation of the deteriorating functions $\varepsilon_{su} = \varepsilon_{su}(\delta_s)$ and $f_c = f_c(\delta_s)$, as well as the numerical validation against experimental results of the damage model adopted in this study, can be found in Biondini and Vergani (2015). Deterioration of concrete is not considered as a critical factor for the applications presented in this article and is hence neglected.

Lifetime seismic assessment of spatially distributed RC bridges

Seismic capacity and bridge damage states

The lifetime seismic capacity of RC bridges is investigated under uncertainty. The seismic capacity $I_{s,b}$ associated with the s-th damage limit state of the b-th bridge in the network depends on the bridge age $t_b = t_0 - t_{c,b}$, where t_0 is the occurrence time of the seismic event and $t_{c,b}$ is the bridge construction time $t_{c,b} < t_0$ (Capacci & Biondini, 2018b) and is hence time-variant due to structural deterioration (Biondini et al., 2014, 2015a; Capacci et al., 2016). The corresponding time-variant fragility curves $P^E_{s,b} = P(I_{s,b}(t_b) \leq i_b)$ provide the probability of exceedance of a damage limit state s_b given the occurrence at time t_0 of a seismic event of intensity i_b at the b-th bridge location.

Fragility curves can be developed using a variety of methods based on static and dynamic structural analyses (Billah & Alam, 2015). In this article, probabilistic nonlinear IDA is used to evaluate the bridge seismic capacity (Vamvatsikos & Cornell, 2002). Time-variant IDA is carried out at different bridge ages taking into account the progressive reduction of the reinforcement mass and ductility. Even though IDA is computationally expensive, it provides a thorough understanding of the structural response of RC bridges, taking into account the uncertainties associated with the ground motion and the degradation of the structural performance (Elnashai & Di Sarno, 2008).

The peak ground acceleration (PGA) is assumed as seismic intensity measure i_b. Limit states should be informed by damage limitation associated with the accumulation of excessive plastic strains in critical regions. As an example, girder bridges under seismic loading are expected to develop plastic hinges at the pier ends. Bridge performance levels can therefore be defined with respect to inelastic displacement demand ratios similarly to what has been developed for buildings (Structural Engineers Association of California [SEAOC], 1995), as proposed in Biondini et al. (2014). A damage measure associated with the maximum pier drift $\theta_{\max,b}$, defined as the largest ratio of the bridge pier top displacement to the pier height experienced during the seismic event, is hence considered in this article. It is worth noting that, depending on the type of structure and failure conditions, multiple critical members and related damage measures can be considered for the definition of limit states and easily incorporated in the proposed framework.

In the following, the attainment of damage states s_b is associated with the following drift thresholds $\theta_{s,b}$ (Capacci, 2015):

- Slight Damage (SD, $s_b = 1$): $\theta_{s=1,b} = \theta_{y,b}$;
- Moderate Damage (MD, $s_b = 2$): $\theta_{s=2,b} = \theta_{y,b} + 0.3\theta_{p,b}$;
- Extensive Damage (ED, $s_b = 3$): $\theta_{s=3,b} = \theta_{y,b} + 0.6\theta_{p,b}$.

with $\theta_{p,b} = \theta_{u,b} - \theta_{y,b}$, and where $\theta_{y,b}$ and $\theta_{u,b}$ are damage measures associated with the first yielding and ultimate bending curvatures, respectively, at the base cross-section of the bridge piers. In addition, the bridge suffers No Damage (ND, $s_b = 0$) if $\theta_{\max,b} < \theta_{1,b}$, and reaches the limit state of Structural Collapse (SC, $s_b = 4$) when the dynamic equilibrium under ground motion is no longer fulfilled. Table 1 defines the set of damage states herein presented and the related limit conditions. The deterioration process induces a progressive reduction of strength, stiffness and ductility of the member cross-section affecting the structural response parameters that originate unacceptable plastic strains at the sectional level (Biondini et al., 2014, 2015a). Therefore, also the damage thresholds should be time-variant: the reference damage measures $\theta_{y,b}(t_b)$ and $\theta_{u,b}(t_b)$ are assessed as the mean values of a probabilistic time-variant non-linear static (pushover) analysis evaluated at different bridge ages (Capacci et al., 2016).

Damage states s_b are associated with seismic capacities $I_{s,b}$. The definition of the drift thresholds $\theta_{s,b}$ obtained from push-over analysis for $s_b = 1,2,3$, ensures $I_{1,b} \leq I_{2,b} \leq I_{3,b}$. With reference to SC limit state $s_b = 4$, it is assumed $I_{s,b} \leq I_{4,b}$ for $s_b = 1,2,3$. Therefore, damage states associated with seismic capacities $I_{s,b}$ are mutually exclusive and collectively exhaustive events (Ang & Tang, 2007) and their

Table 1. Definition of damage states and limit conditions.

Damage state	Acronym	s_b	Limit condition
No damage	ND	0	$\theta_{\max,b} < \theta_{y,b}$
Slight damage	SD	1	$\theta_{\max,b} \geq \theta_{y,b}$
Moderate damage	MD	2	$\theta_{\max,b} \geq \theta_{y,b} + 0.3\theta_{p,b}$
Extensive damage	ED	3	$\theta_{\max,b} \geq \theta_{y,b} + 0.6\theta_{p,b}$
Structural collapse	SC	4	Loss of dynamic equilibrium

probability of occurrence can be defined as follows:

$$\begin{cases} P_{s=0,b} = P(s_b = 0) = P(I_{1,b} < i_b) \\ P_{s=1,b} = P(s_b = 1) = P(I_{2,b} < i_b \le I_{1,b}) \\ P_{s=2,b} = P(s_b = 2) = P(I_{3,b} < i_b \le I_{2,b}) \\ P_{s=3,b} = P(s_b = 3) = P(I_{4,b} < i_b \le I_{3,b}) \\ P_{s=4,b} = P(s_b = 4) = P(I_{4,b} \ge i_b) \end{cases} \quad (4)$$

Assuming perfect linear correlation between each pair of fragility curve and setting $P^E{}_{0,b} = 1$ and $P^E{}_{5,b} = 0$, the time-variant probability of occurrence of the damage state $s_b = 0, \ldots, 4$ on the b-th bridge can be conveniently reduced to the following compact form

$$P_{s,b} = P^E_{s,b} - P^E_{s+1,b} \quad (5)$$

Earthquake scenario and seismic demand

The seismic risk assessment of vulnerable structures, however, should be informed by several critical factors, including the uncertain distance from the site of the earthquake source (Cornell, 1968). The seismic demand of spatially distributed bridges can be evaluated by ground motion prediction equations (GMPEs). Based on GMPEs, seismic intensity $i_b = i_b(d_{e,b}, M)$ at the site of the b-th bridge in the network is related to both earthquake magnitude M and source-to-site distance $d_{e,b}$, which is the distance between the epicentre location $\mathbf{x}_e$ and the bridge site $\mathbf{x}_b$.

Furthermore, area sources are often used in practice to account for 'background' seismicity (Baker, 2009) and they can model the seismic exposure of regions characterised by lack of information on the local active faults. Assuming that the likelihood of occurrence of a seismic event with given magnitude is equal in any point along the area source A_s, the uniform probability density function associated with the epicentre location can be expressed as follows

$$f_{X_e}(\mathbf{x}_e) = \frac{I(\mathbf{x}_e)}{A_s} \quad (6)$$

where $I(\mathbf{x}_e)$ is a step function with $I(\mathbf{x}_e) = 1$ if the epicentre location lies within the area source, i.e. $\mathbf{x}_e \in A_s$, and $I(\mathbf{x}_e) = 0$ otherwise.

Damage combinations probability and hazard capacity vectors

The emergency response to hazardous events of complex systems such as critical infrastructures is affected by the damage state combination of a large number of vulnerable network components. In practical applications, the seismic reliability assessment of bridge networks can be carried out based on simulation techniques (Ghosh, Rokneddin, Padgett, & Dueñas-Osorio, 2014) or analytical methods relying on suitable mathematical formulations (Kang, Song, & Gardoni, 2008). Assessing the vulnerability of a large-scale network can be a challenging task not only due to the computational costs, but also due to incomplete information on the bridge vulnerability and on their statistical dependence (Der Kiureghian & Song, 2008; Song & Ok, 2010). In order to focus on the methodological aspects of the time-variant metrics of seismic resilience proposed in the article, the applications will deal with simple small-scale networks.

Based on the ordered selection with repetitions of the damage states s_b for each bridge in a given road system, network damage combinations can be associated with the following integer index s

$$s = 1 + \sum_{b=1}^{N_b} (N_{s,b})^{N_b - b} \cdot s_b \quad (7)$$

where N_b is the number of bridges in the network and $N_{s,b}$ is the number of possible damage states for the b-th bridge. Consistently with the set of possible damage states of a single bridge, all the possible network damage combinations represent a set of mutually exclusive and collectively exhaustive events. In particular, the event $s = 1$ refers to the undamaged network condition ($s_b = 0, \forall b$) and the combination associated with all bridges suffering the most severe damage is $s = N_s$, which is the total number of possible network damage combinations

$$N_s = \prod_{b=1}^{N_b} N_{s,b} \quad (8)$$

The time-variant structural capacities of the reference set of vulnerable facilities under interdependent hazards, such as the seismic scenario and age-induced deterioration process, are collected in a hazard capacity vector $\boldsymbol{\eta}$. The time-variant probability of occurrence of the s-th network damage combination $P_s = P(s|\boldsymbol{\eta})$ is conditioned by several factors collected in $\boldsymbol{\eta}$ associated with the seismic demand and structural capacity of the spatially distributed vulnerable bridges in the network. In general, the network damage combinations depend on the seismic intensity i_b at the b-th bridge location, bridge age t_b and correlation between the seismic capacities associated with each damage state and each pair of bridges in the network. Therefore, the conditional probabilities can be defined in terms of the intensity-based vector $\boldsymbol{\eta}_i$

$$\boldsymbol{\eta}_i = \{i_b, t_b, \boldsymbol{\rho}\} \quad (9)$$

where $\boldsymbol{\rho}$ is the matrix of the linear correlation coefficients of each pair of seismic capacities (Capacci & Biondini, 2018b). However, for spatially distributed bridges, the seismic intensities i_b are related to the earthquake scenario in terms of magnitude M, epicentre location $\mathbf{x}_e$ and bridge site $\mathbf{x}_b$. In this case, a pointwise hazard capacity vector $\boldsymbol{\eta}_e$ needs to be introduced

$$\boldsymbol{\eta}_e = \{M, \mathbf{x}_e, \mathbf{x}_b, t_b, \boldsymbol{\rho}\} \quad (10)$$

As mentioned, a seismic area source A_s may be conveniently used in practice to model the seismic exposure of entire regions. In this case, the conditional probabilities associated with network damage combinations can be evaluated based on the total probability theorem as follows

$$P_s(s|\boldsymbol{\eta}_A) = \int_{A_s} P_s(s|\boldsymbol{\eta}_e) \cdot f_{X_e}(\mathbf{x}_e) \cdot dA \tag{11}$$

where an area-based hazard capacity vector $\boldsymbol{\eta}_A$ is defined in terms of the area source A_s

$$\boldsymbol{\eta}_A = \{M, A_s, \mathbf{x}_b, t_b, \boldsymbol{\rho}\} \tag{12}$$

Traffic flow analysis of road networks

Congestion-based traffic model

The performance and functionality of road networks can be assessed based on traffic flow response and minimum travel time given origin-destination (O-D) traffic demands and network topology (Bocchini & Frangopol, 2011). A road arc is defined by the origin i, where the flow gets into the arc, and the destination j, where the users get out of the arc. The travel time c_{ij} of the arc $i-j$ can be expressed as a function of several parameters: $c_{ij} = c_{ij}(f_{ij};L_{ij},n_L,d_{\min},v_{cr},v_{lim})$, where: f_{ij} is the traffic flow of vehicles per unit of time in the arc $i-j$; L_{ij} and n_L are, respectively, the arc length and number of open lanes of each road arc; $d_{\min}$, v_{cr} and v_{lim} are, respectively, the minimum allowed distance between vehicles, the speed associated with critical capacity (i.e. the critical speed) and the speed limit for each road class. It is worth noting that when the arc includes vulnerable bridges along the network, the travel time spent to cross it also depends on the post-earthquake conditions of each damaged structure.

Among all lifelines, transportation networks have a unique feature: all nodes can be both an origin and a destination of traffic flows. In this study, the two-way traffic flows for all road users incoming and outgoing the highway network are prescribed a priori, based on literature data. However, it is worth noting that the O-D traffic flows can also be related to the condition of the network. As an example, after seismic events, due to the damages of the transportation infrastructure system, the users may adapt their trips preferring closer destinations (Bocchini & Frangopol, 2011), changing the travel mode or even eliminating scheduled activities suppressing trips (Erath, Birdsall, Axhausen, & Hajdin, 2009). Furthermore, the emergency vehicles demand should vary over time according to the actual emergency response of the affected region.

Road arc travel time

According to Bocchini and Frangopol (2011), the travel time c_{ij} is related to the traffic flow f_{ij} as follows

$$c_{ij} = c_{ij}^0 \left[1 + \alpha \left(\frac{f_{ij}}{f_{ij}^{cr}}\right)^{\beta}\right] \tag{13}$$

with $\alpha = 0.15$ and $\beta = 4$ (Bocchini & Frangopol, 2012b; Martin & McGuckin, 1998). The travel time at free flow ${c^0}_{ij} = L_{ij}/v_{lim}$ is the time spent by one car to cross the arc with no traffic, and the practical capacity $f_{ij}^{cr} = n_L(v_{cr}/d_{lim})$ is the critical flow capacity at which the congestion starts to heavily affect the traffic (for $f_{ij} > f_{ij}^{cr}$ the travel time increases with higher rate).

The traffic capacity of a road arc may be impaired by traffic restrictions applied to regulate the transit on damaged bridges (Mackie & Stojadinović, 2006). A generic arc can involve $N_{ij,f}$ free segments and $N_{ij,b}$ bridges. Therefore, the travel time c_{ij} of the O-D arc will be the sum of the travel time $c_{ij,f}$ for each free segment and $c_{ij,b}$ each bridge

$$c_{ij} = \sum_{f=1}^{N_{ij,f}} c_{ij,f} + \sum_{b=1}^{N_{ij,b}} c_{ij,b} \tag{14}$$

To reduce the computational cost, it is possible to define an equivalent arc that incorporates the traffic response of each bridge crossing the road segment. The travel time c_{ij} of the equivalent arc is defined as a function of the traffic flow f_{ij} based on the following definitions for ${c^0}_{ij}$ and ${f^{cr}}_{ij}$ (Bocchini & Frangopol, 2012a)

$$c_{ij}^0 = \sum_{f=1}^{N_{ij,f}} c_{ij,f}^0 + \sum_{b=1}^{N_{ij,b}} c_{ij,b}^0 \tag{15}$$

$$f_{ij}^{cr} = \beta \sqrt{\frac{c_{ij}^0}{\sum_{f=1}^{N_{ij,f}} \frac{c_{ij,f}^0}{\left(f_{ij,f}^{cr}\right)^{\beta}} + \sum_{b=1}^{N_{ij,b}} \frac{c_{ij,b}^0}{\left(f_{ij,b}^{cr}\right)^{\beta}}}} \tag{16}$$

Total travel time and optimal traffic flows

The actual traffic flow distribution in each road of the highway network can be identified based on the user-equilibrium condition enforced by Wardrop's gravitational model (Wardrop, 1952). This condition consists in minimising the total travel time (TTT), i.e. the time spent by all users to reach any destination from any origin departing in a fixed time window. The TTT is computed as follows (Bocchini & Frangopol, 2011):

$$\mathrm{TTT} = \sum_{i \in I} \sum_{j \in J} \int_0^{f_{ij}} c_{ij}(f) df \tag{17}$$

where f is a dummy integration variable, I is the set of all the generic nodes in the network and J is the subset of nodes connected to node i by a road segment.

Therefore, an optimisation problem needs to be solved. In this study, the enforcement of user-equilibrium condition relies on a suitable implementation of the Frank–Wolfe algorithm (Frank & Wolfe, 1956). Given the O-D traffic demand and the arc parameters, the optimisation procedure exploits the convexity of the solution domain (Evans, 1976) to define a sequence of feasible solutions in terms of traffic flow distribution f_{ij} that converges to the optimal one (i.e. the one satisfying the user-equilibrium condition). More details can be found in Bocchini and Frangopol (2011) and Capacci (2015).

Life-cycle seismic resilience of road networks

Bridge traffic limitations

The actual practicability of each arc depends on the set of restrictions that the owner of the transportation network imposes to regulate the traffic along each bridge damaged by hazardous events. Restrictions to each type of vehicle and limitations to traffic network capacity are applied depending on the damage state of the bridges in the road network (Mackie & Stojadinović, 2006).

The type of users of road networks depends on the needs and duties associated with travels. Three different types of road users are considered to define the O-D demand: light vehicles f_l, heavy vehicles f_h, and emergency vehicles f_e. Traffic limitations on the b-th bridge are identified by a decision variable d_b based on the following $N_{d,b} = 5$ traffic restrictions (Biondini et al., 2015a):

- No restrictions ($d_b = 0$): the traffic on the bridge is regular and the speed limit v_{lim} corresponds to the maximum allowed speed $v_{\max}$.
- Weight restriction ($d_b = 1$): heavy vehicles are forbidden, i.e. $f_h = 0$, and the speed limit is reduced to $v_{\min}$.
- One lane open only ($d_b = 2$): light and emergency vehicles can transit on only one lane, i.e. $n_L = 1$.
- Emergency access only ($d_b = 3$): the transit of emergency vehicles only is allowed, i.e. $f_l = 0$.
- Closure ($d_b = 4$): no vehicles can transit over the bridge, i.e. $f_e = 0$ or $n_L = 0$.

Network traffic combinations and functionality

The set of possible states of the bridge decision variable d_b considered in this article are listed in Table 2, where the restrictions $d_b = k$ with $k > 1$ are inclusive of the traffic limitations associated with $d_b < k$. Each network restriction combination d and the number of possible combinations N_d can be expressed in terms of the decision variable d_b of each bridge consistently with the criterion proposed for the damage state combinations

$$d = 1 + \sum_{b=1}^{N_b} (N_{d,b})^{N_b - b} \cdot d_b \tag{18}$$

$$N_d = \prod_{b=1}^{N_b} N_{d,b} \tag{19}$$

The functionality level $Q_d(d) \in [0;1]$ of the road network associated with the combination d of traffic restrictions is defined as follows (Capacci, 2015)

$$Q_d = \frac{\mathrm{TTT}_u}{\mathrm{TTT}_d(d)} \tag{20}$$

where $\mathrm{TTT}_d = \mathrm{TTT}(d)$ is the total travel time when the d-th network restriction combination is applied and $\mathrm{TTT}_u = \mathrm{TTT}(d = 1)$ is the total travel time under unrestricted conditions, i.e. no traffic regulations are applied to any bridge. The condition of unrestricted transit with $\mathrm{TTT}_d = \mathrm{TTT}_u$ and $Q_d = 1$ holds for the network with all bridges under no damage state. Such condition is fulfilled before the occurrence of significant structural deterioration or seismic damage and after recovery processes with bridges fully restored.

Table 2. Definition of decision variables and traffic limitations.

Decision variable	d_b	Traffic limitation
No restrictions	0	$v_{\lim} = v_{\max}$ and $n_L =$ bridge lanes
Weight restriction	1	$f_h = 0$ and $v_{\lim} = v_{\min}$
One lane open only	2	$n_L = 1$
Emergency access only	3	$f_l = 0$
Closure	4	$f_e = 0$ or $n_L = 0$

Bridges may suffer a loss of structural capacity when an earthquake occurs. The initial restrictions in the aftermath of the occurrence of the seismic event are associated with the attainment of the limit states for each bridge in the network. In particular, the traffic restriction $d_b = k$ is applied to the b-th bridge if the earthquake induces the damage state $s_b = k$. Therefore, a seismic event would cause a sudden drop of network functionality from the pre-event level to $Q_{s=d}$ due to the traffic restrictions under the initial damage combination s.

Recovery process of bridge structural capacity

After the occurrence time t_0, the repair activities of each given bridge in the network will start at the idle time $t_{i,b}$ and will be carried out up to the recovery time $t_{r,b}$ (i.e. the time of repair completion). The purpose of post-event repair actions is to restore partially or totally the pre-event seismic capacity of the bridges in the network to ensure the safety of the roadway users. The structural recovery profile depends on several factors, including type of system and components, magnitude and location of damage, and restoring techniques (Bocchini, Decò, & Frangopol, 2012; Decò et al., 2013). Effective functionality recovery models have been proposed by Kafali and Grigoriu (2005), Cimellaro et al. (2010b), Bocchini et al. (2012), Titi and Biondini (2013), Karamlou and Bocchini (2017a, 2017b), Sharma, Tabandeh, and Gardoni (2018). The following recovery model $r_b = r_b(\tau) \in [0;1]$ is adopted over the bridge recovery time interval $\Delta t_{r,b} = t_{r,b} - t_{i,b}$ (Titi et al., 2015)

$$r_b(\tau) = \begin{cases} 0 & ,\tau \le 0 \\ \omega^{1-\psi}\tau^{\psi} & ,0 < \tau \le \omega \\ 1-(1-\omega)^{1-\psi}(1-\tau)^{\psi} & ,\omega < \tau \le 1 \\ 1 & ,\tau > 1 \end{cases} \tag{21}$$

where $\tau = (t - t_{i,b})/\Delta t_{r,b} \in [0,1]$ is a normalised time variable.

The parameters $\omega \in [0,1]$ and $\psi \ge 0$ define the shape of the recovery profile. A proper calibration of the shape parameters for each bridge in the networks allows to effectively reproduce continuous recovery processes, for example in limit cases where functionality is restored quickly after the seismic event ($\omega \approx 0$ and $\psi > 1$), gradually in time ($\psi \approx 1$), or mainly at the end of the recovery process ($\omega \approx 1$, $\psi > 1$). The type of recovery actions and, consequently, the values of the shape parameters should be selected depending on the damage state to be restored and on the related effectiveness of the repair activities. The calibration of recovery

models of each damaged bridge in the network based on all the variables involved and their uncertainties is out of the scope of the article.

Recovery process of network functionality

Post-event repair activities on each bridge lead to a progressive network functionality restoration. The road network functionality is described by a discrete set of values as a function of the damage state of the bridges and the limit states progressively restored at the component level (Padgett & DesRoches, 2007). Therefore, the repair activities on each bridge lead to the definition of a constant stepwise model for network functionality, evolving from the initial damage combination up to the traffic restrictions at repair completion.

The recovery process of each bridge initiates after an idle time $t_{i,b}$ and develops over a series of time steps. The partial recovery times $t_{p,b}$ are related to time instants in which the attainment of intermediate structural capacity targets r_p allows the enforcement of less severe traffic limitations up to complete reopening of the bridge to all users. In particular, $p = 1, \ldots, N_{j,b}$ where $N_{j,b}$ is the total number of steps in the network recovery process induced by restoration of the b-th bridge. The completion of the repair actions on the b-th bridge is reached at the final recovery time $t_{r,b}$. According to the bridge structural recovery model, partial and final recovery times of each bridge depend not only on the initial damage state s_b, and on the intermediate capacity targets r_p, but also on the specific repair strategy applied to restore the bridge structural capacity. In the following it is assumed that the initial traffic limitations $d_b = k$ with $k > 0$ are partially released through a progressively decreasing sequence of less severe restrictions $d_b = h$ with $k < h$. Finally, full serviceability of the bridge, i.e., $d_b = 0$, is assumed to be reached at $t_{r,b}$.

The recovery function of network functionality over the horizon time interval $\Delta t_h = t_h - t_0$ between the occurrence time t_0 and a given horizon time t_h is hence defined in stepwise form as follows:

$$Q(t) = Q_j, \quad t_j \le t < t_{j+1} \forall j \in [0, N_j] \tag{22}$$

where t_j is the time instant associated with a partial or total recovery time of a bridge in the network and Q_j is the network functionality after the j-th step over the time interval $\Delta t_j = t_{j+1} - t_j$, i.e. the recovery time interval. The total number of time steps in the network recovery process is defined as $N_j = \sum_b N_{j,b}$, with $t_h = t_{j+1}$ for $j = N_j$.

In this article, the recovery process is assumed to be prescribed based on the post-earthquake damage state of each individual bridge. Optimal planning of the recovery interventions is not investigated. However, prioritising the interventions on individual bridges is necessary for effective emergency management strategies under limited resources.

Time-variant seismic resilience

The resilience level R_s associated with the network damage combination s is defined as the average integral of the network functionality over the horizon time interval Δt_h

$$R_s = \frac{1}{\Delta t_h} \int_{t_0}^{t_h} Q(t) dt \tag{23}$$

Given the stepwise form of the recovery profile, the average integral can be expressed in summation form as follows

$$R_s = \frac{1}{\Delta t_h} \sum_{j=0}^{N_j} Q_j \cdot \Delta t_j \tag{24}$$

The recovery phase and pattern of network functionality are related to the repair activities carried out to restore each bridge in the road system from the given post-event damage state combination. Severe seismic damage and late restoration can substantially reduce the network resilience. In fact, the application of restrictive traffic limitations may force traffic flows to be detoured to secondary roads for the time interval required to carry out the necessary repair activities. These effects could be mitigated by upgrading interventions aimed at improving the network connectivity by means of new road branches and alternative travel paths, which may provide significant gains in seismic resilience (Biondini et al., 2017; Capacci & Biondini, 2018a). In this context, the resilience levels depend on both the network layout, in terms of the related functionality levels Q_d, and variables affecting the recovery from the s-th damage state combination, which can conveniently be collected in a capacity recovery vector $\boldsymbol{\gamma}_s$.

A comprehensive quantification of resilience is herein presented and inspired by the concept of expected utility (Ang & Tang, 1984). The proposed resilience measure R is obtained by weighing the resilience levels R_s of the N_s network damage combinations with the corresponding probabilities of occurrence conditioned by the variables collected in the hazard capacity vector $\boldsymbol{\eta}$

$$R(\boldsymbol{\eta}, \boldsymbol{\gamma}, Q_d) = \sum_{s}^{N_s} P_s(s|\boldsymbol{\eta}) \cdot R_s(\boldsymbol{\gamma}_s, Q_d) \tag{25}$$

where $\boldsymbol{\gamma}$ collects the information contained in $\boldsymbol{\gamma}_s$ for any damage combination s. The type of resilience measure depends on the definition of damage probabilities through the hazard capacity vector $\boldsymbol{\eta}$. The following measures are considered

- Intensity-based resilience $R = R(i_b)$ based on $\boldsymbol{\eta}_i$; this measure is convenient for road networks with a single bridge exposed to seismic events with intensity i_b.
- Pointwise resilience measure $R = R(M, \mathbf{x}_e)$ associated with $\boldsymbol{\eta}_e$, which depends on the earthquake scenario in terms of magnitude M and epicentre location $\mathbf{x}_e$ and it may be used for road networks with spatially distributed bridges.
- Area-based resilience measure $R_A = R_A(M, A_s)$ associated with $\boldsymbol{\eta}_A$; this is an average measure for seismic events

with earthquake magnitude M and epicentre located within a prescribed seismic area source A_s. It provides a more synthetic measure of resilience for road networks with spatially distributed bridges.

Applications

The effectiveness of the proposed approach is shown through three case studies focusing on assessing the seismic resilience of road networks with RC bridges, evaluating the effects of structural deterioration associated with corrosion, and investigating the role of spatial distribution of vulnerable bridges, respectively.

The first case study is devoted to the seismic resilience assessment of simple networks with only one RC bridge. The fragility curves of the bridge are evaluated considering two different types of pier cross-section to emphasise the role of both the bridge structural capacities and recovery processes from seismic damage. The second case study is aimed at investigating the detrimental effects of bridge aging and deterioration on the lifetime seismic resilience of different road networks. Finally, two road networks with spatially distributed bridges are considered in the third case study to show the influence of both the earthquake scenario and environmental aggressiveness on the network resilience.

RC bridge

The four-span continuous RC bridge shown in Figure 1 is considered (Pinto et al., 1996; Titi et al., 2015). The total length of the bridge deck is 200 m, with four spans of 50 m each. The box girder cross-section is shown in Figure 2(a). Two different configurations of the bridge piers are considered: hollow-core rectangular box cross-section with height $H = 21$ m (Figure 2(b)) and circular cross-section (Mander, Dhakal, Mashiko, & Solberg, 2007) with height $H = 14$ m (Figure 2(c)). The nominal material properties are as follows: concrete compression strength $f_c = 40$ MPa; steel yielding strength $f_{sy} = 450$ MPa; concrete ultimate strain in compression $\varepsilon_{cu} = 0.35\%$; steel ultimate strain $\varepsilon_{su} = 7.5\%$.

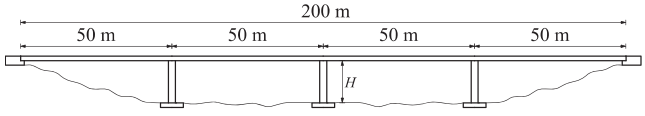

Figure 1. Four-span continuous RC box-girder bridge.

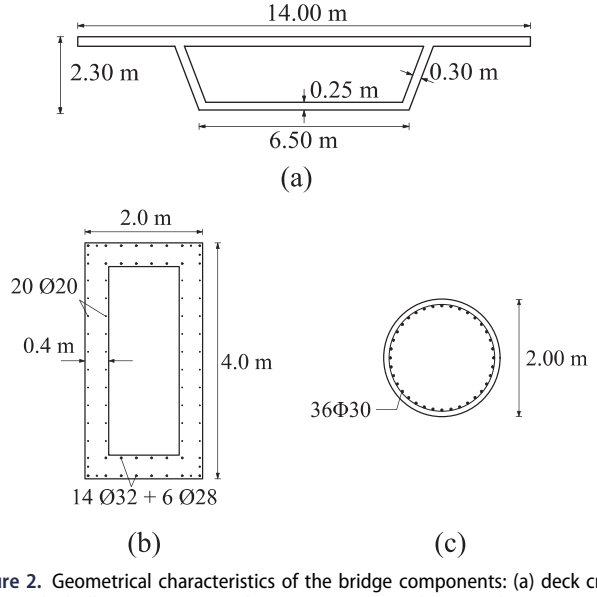

Figure 2. Geometrical characteristics of the bridge components: (a) deck cross-section; (b) hollow-core rectangular cross-section, and (c) circular cross-section of the piers.

The piers are exposed to chloride diffusive attack on the external surface, with nominal concentration $C_0 = 3\%$ [wt.%/c]. A nominal diffusivity coefficient $D = 15.8 \times 10^{-12}$ m^2/sec is assumed. The corrosion damage is evaluated by assuming a nominal damage rate coefficient $q_s = (0.02\,\text{year}^{-1})/C_0$, with corrosion initiation associated with a nominal critical concentration $C_{cr} = 0.6\%$ [wt.%/c] (fib, 2006).

Structural modelling and seismic analysis

The seismic performance of multispan RC girder bridges have been studied in previous works under different assumptions regarding the abutments and soil structure interaction (Isaković & Fischinger, 2000; Ni, Petrini, & Paolucci, 2014). In this article, such issues are not investigated and a structural model with roller supports at the abutments and piers with fixed ends is assumed. The structural model is developed with a level of complexity that allows capturing the dominant behaviour of the bridge and, at the same time, limit the computational cost of the probabilistic analysis.

The deck is modelled by elastic beam elements. Under transversal loading, plastic hinges are expected to develop only at the pier ends (Biondini et al., 2014; Priestley, Calvi, & Kowalsky, 2007). The piers are hence modelled through beam elements with lumped plasticity. The nonlinear behaviour of the plastic hinges is defined in terms of bending moment versus curvature relationship based on the Mander model for concrete (Mander, Priestley, & Park, 1988) and a bilinear elastic-plastic model for reinforcing steel. The hysteretic behaviour is based on the Takeda model (Takeda, Sozen, & Nielsen, 1970), with a backbone curve defined by a stepwise linearisation of the moment versus curvature diagram. The length of the plastic hinge is evaluated as proposed by Paulay and Priestley (1992).

Seismic analysis is carried out considering a uniform gravity load equal to 315 kN/m, including self-weight, dead loads and a 20% of live loads, applied on the deck. Non-linear time-history dynamic analyses of the RC bridge are performed using OpenSees (Mazzoni, McKenna, Scott, Fenves, et al., 2006).

Probabilistic model

The uncertainties associated with the structural system and the aging process is taken into account based on a set of mechanical and environmental parameters modelled as uncorrelated random variables. These parameters are:

Table 3. Probability distributions and coefficients of variation (μ = mean value).

Random variable (t = 0)	Distribution type	C.o.V.
Concrete strength, f_c	Lognormal	5MPa/μ
Steel strength, f_{sy}	Lognormal	30MPa/μ
Viscous damping, ξ	Normal*	0.40
Diffusivity, D	Normal*	0.20
Damage rate, q_s	Normal*	0.30
Chloride concentration, C_0	Normal*	0.30
Critical concentration, C_{cr}	Beta**	0.25

*Truncated distributions with non-negative outcomes.
**Lower bound b_{min} = 0.2 wt.–%/c; Upper bound b_{max} = 2.0 wt.–%/c.

concrete compression strength f_c; steel yielding strength f_{sy}; viscous damping ξ; diffusivity coefficient D; damage rate q_s; chloride concentration along the pier circular cross-section C_0; critical concentration C_{cr}. Nominal values are assumed as mean values. The analytical models for the distribution of the considered random variables and their coefficients of variation are listed in Table 3 (Biondini et al., 2006; Dolšek, 2009). The variability of the ground motion is accounted for by considering a set of ten artificial earthquakes (SIMQKE, 1976) generated to be compatible with the elastic response spectrum given by Eurocode 8 for soil type B (CEN-EN 1998-1, 2004).

The life-cycle fragility analysis is carried out based on 1000 samples resulting from the application of each artificial accelerogram to 100 realisations of the deteriorating bridge by means of Monte Carlo simulation and Latin Hypercube Sampling (Iman & Conover, 1982) with correlation control based on Simulated Annealing (Vořechovský & Novák, 2009). The sample size has been selected as a trade-off between computational effort and representativeness of the uncertainties involved in seismic demand, seismic capacity, and structural deterioration (Capacci, 2015). The IDA realisations are processed at different bridge ages by assuming time-variant lognormal distribution of the seismic fragilities

$$P^{E}_{s,b}(i_b, t_b) = P(I_{s,b}(t_b) \le i_b) = \Phi\left(\frac{\ln i_b - \lambda_{s,b}(t_b)}{\zeta_{s,b}(t_b)}\right) \qquad (26)$$

where Φ refers to the cumulative distribution function of the standard normal variate, and $\lambda_{s,b}$ and $\zeta_{s,b}$ are the mean and standard deviation, respectively, of the natural logarithm of the seismic capacity $I_{s,b}$ associated with damage state s_b.

Lifetime fragility analysis of the RC bridge under corrosion

The results of the probabilistic IDA at the initial time, with no corrosion, are shown in Figure 3 for both types of bridge piers in terms of median, 16% and 84% IDA capacity curves (Vamvatsikos & Cornell, 2002). The probability of exceeding a prescribed limit state given the intensity measure i_b corresponding to the PGA is described by means of fragility curves. Figure 4 shows the lognormal best fitting of the fragility curves for the four investigated limit states s_b = 1,2,3,4, from slight damage up to collapse. The drift

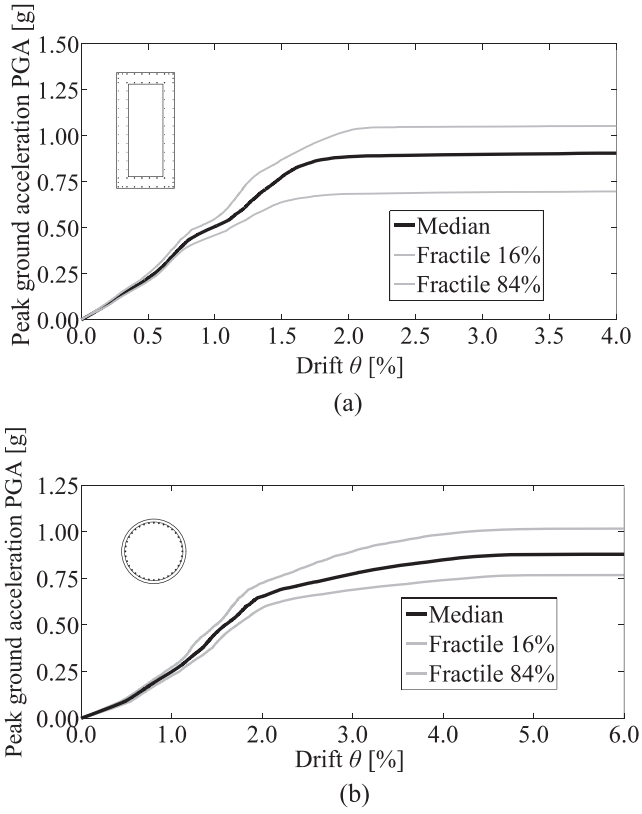

Figure 3. Probabilistic parameters of the IDA capacity curves (median, 16% and 84% fractiles) of the RC bridge: piers with (a) hollow-core rectangular cross-section and (b) circular cross-section.

thresholds associated with each intermediate damage state are collected in Table 4.

The fragility curves are then used to compute the bridge damage probabilities for a given seismic demand shown in Figure 5, which are the weighting coefficients of the intensity-based resilience measure associated with the hazard capacity vector $\boldsymbol{\eta}_i$. In particular, the curve associated with $s_b = 4$ (i.e., probability of 'Structural Collapse') corresponds to the fragility curve associated with the most severe damage state and the curve associated with $s_b = 0$ (i.e., probability of 'No Damage') represents the complementary CDF of the least severe damage state (i.e., 'Slight Damage'). It is worth noting that the bridge vulnerability to slight damage is almost the same for both types of bridge piers. However, the larger flexibility due to the slenderness of bridge pier with circular cross-section along with the higher sectional ductility guaranteed by the confinement (Capacci, 2015) provides a better seismic response in the post-elastic range (especially for MD and ED limit state) with respect to hollow-core rectangular cross-section bridge piers.

The effects of a severe environmental exposure scenario on the time-variant seismic performance of the RC bridge are displayed in Figures 6 and 7 for the case of piers with circular cross-section (Figure 3(c)). A similar trend qualitatively holds also for the case of piers with hollow-core rectangular cross-section. Figure 6 represents the time-variant drift thresholds associated with each intermediate limit state for the bridge with circular piers, based on the outcomes of the pushover analyses in terms of first yielding drift $\theta_{y,b} = \theta_{1,b}$ and ultimate drift $\theta_{u,b}$.

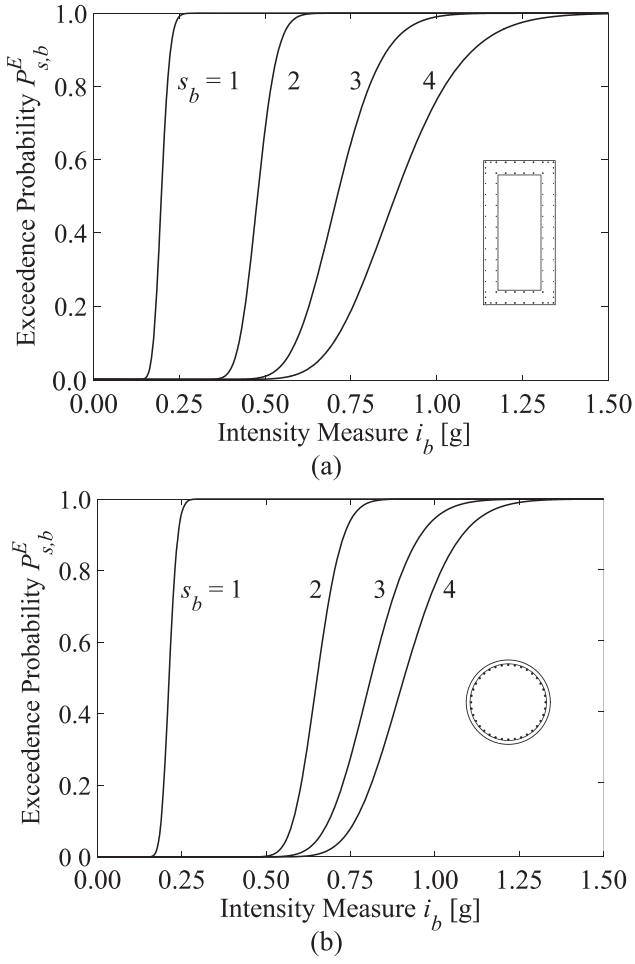

Figure 4. Lognormal model of the fragility curves of the RC bridge: piers with (a) hollow-core rectangular cross-section and (b) circular cross-section.

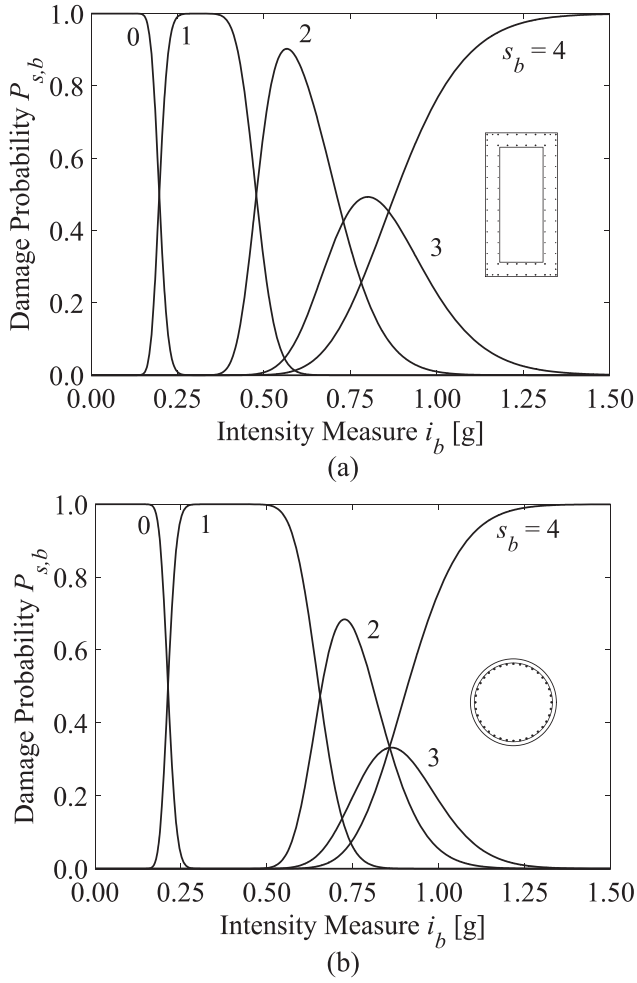

Figure 5. Probability of occurrence of damage state s_b of the RC bridge: piers with (a) hollow-core rectangular cross-section and (b) circular cross-section.

Table 4. Drift thresholds of the RC bridge ($t_b = 0$).

Damage state	$\theta_{s=1,b}$ [%]	$\theta_{s=2,b}$ [%]	$\theta_{s=3,b}$ [%]
Hollow-core rectangular cross-section ($H = 21$m)	0.44	0.92	1.40
Circular cross-section ($H = 14$m)	0.87	2.09	3.31

Figure 7 depicts the lognormal best fitting of the four time-variant fragility curves for different bridge ages t_b every 10 years up to 100 years. Except for the slight damage limit state, the probability of exceedance of each limit state increases over time due to the detrimental effects of corrosion on longitudinal reinforcing steel bar cross-sectional area and steel ductility. The central values of each fragility curve tend to decrease in time, whilst their dispersion slightly tends to decrease after more than 60 years. The extreme environmental conditions assumed in the present application lead to an increase in time of the probability of complete corrosion damage (i.e., $\delta_s \approx 1$), reducing in turn the incidence in the fragility analysis of the random variables associated with the deterioration process.

Resilience of highway networks

Three types of highway road networks, as shown in Figure 8, are investigated (Biondini et al., 2015b). The traffic

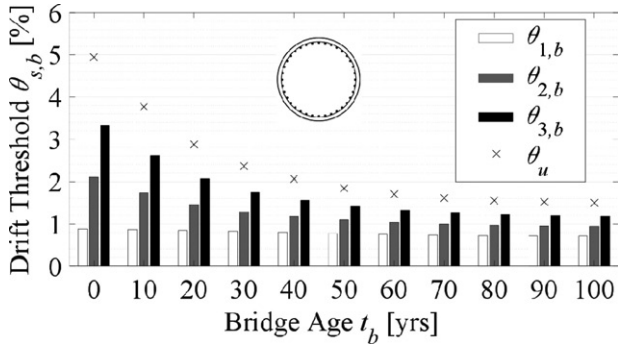

Figure 6. Time-variant drift thresholds associated with different limit states.

parameters of the road segments are summarised in Table 5. Each network is characterised by one origin and one destination, respectively originating and attracting all trips. Three types of road segments define the network topologies and provide the connectivity between the nodes:

- Highway of overall length $L_{ij} = 10$ km, $n_L = 3$ lanes and maximum speed limit $v_{\max} = 130$ km/h. It is the faster route available for the users, but the structural damage of the vulnerable elements may impair its practicability.

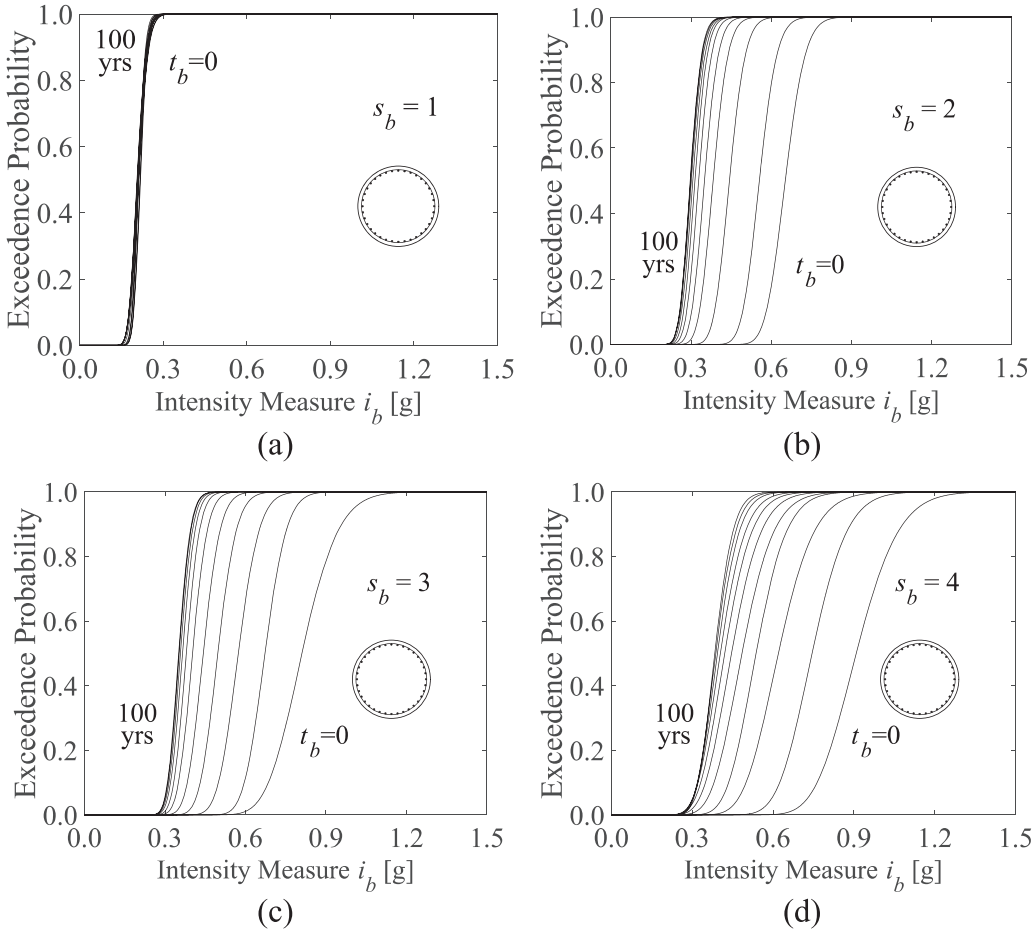

Figure 7. Lognormal model of the time-variant fragility curves for the RC bridge with circular cross-section of the piers under a seismic event occurring at bridge age from t_b every 10 years up to 100 years: (a) slight damage, (b) moderate damage, (c) extensive damage, and (d) structural collapse.

The component B indicated in Figure 8 represents a single bridge. Network N1 is a single road segment.

- Secondary road of overall length $L_{ij} = 40$ km, $n_L = 2$ lanes and maximum speed limit $v_{\max} = 90$ km/h. In the case of network N2, such detour provides a viable alternative to the users when the principal roadway undergoes traffic limitations.
- Re-entry link of length $L_{ij} = 1$ km, $n_L = 1$ lane and same speed restrictions as the secondary road, i.e., $v_{\max} = 90$ km/h. In network N3, the reduction of travel times and distances is mitigated by a prompt return into the main route of the traffic flow rerouted to the secondary road. The topological location of the re-entry link is defined in terms of a dimensionless parameter $\bar{\lambda}$, which expresses the ratio between the distance of the re-entry link from the origin node and the main total length of the highway branch.

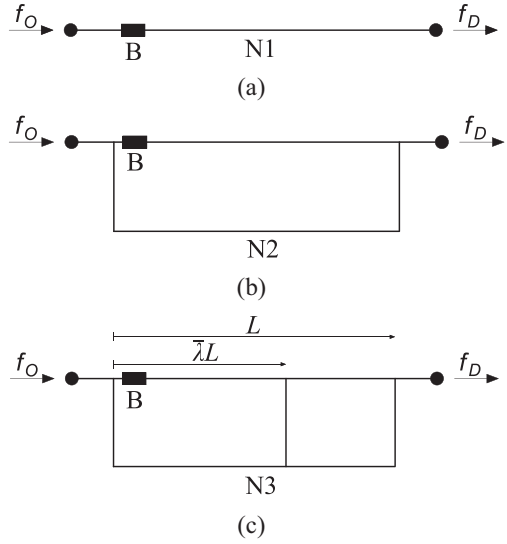

Figure 8. Highway road networks with a single bridge component B: (a) highway with a single road segment (N1); (b) highway with detour (N2); (c) highway with detour and re-entry link (N3).

The two-way traffic flows associated with light, heavy and emergency vehicles are adapted from literature data and assumed as $f_l = 7000$ cars/h, $f_h = 1000$ cars/h and $f_e = 700$ cars/h, respectively. Figure 9 shows the bar chart that collects the functionality levels Q_d of each network given the decision variable d_b associated with the bridge B. These results allow quantifying the drop of network functionality induced by the traffic limitations in terms of network topology and traffic restriction severity. Due to the complete lack of redundancy, any bridge restriction on network N1 leads to its complete inoperability as soon as some road users are not allowed to reach the destination node (from

Table 5. Traffic parameters of the road segments of the highway networks.

Traffic parameters	Highway road	Secondary road	Re-entry link
Length L_{ij} [km]	10	40	1
Number of lanes n_L	3	2	1
Speed limit v_{max} [km/h]	130	90	90
Reduced speed limit v_{min} [km/h]	70	50	50
Critical speed v_{cr} [km/h]	65	65	65
Minimum distance d_{min} [m/cars]	30	30	30

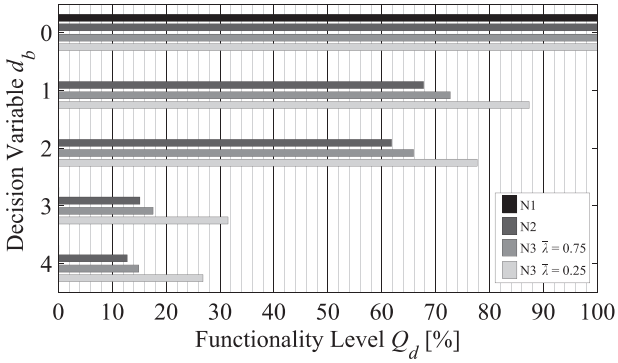

Figure 9. Bar chart of the functionality levels Q_d given the decision variable d_b for networks N1, N2 and N3 with $\bar{\lambda} = 0.25$ and 0.75.

Weight Restriction, $d_b = 1$, up to Closure, $d_b = 4$). The presence of a detour in network N2 guarantees connectivity between origin and destination nodes when traffic limitations are applied, leading to non-zero value even for the minimum functionality level associated with $d_b = 4$. Finally, the higher degree of redundancy of network N3 involves an increase of functionality for each traffic restriction. The mitigation of the impact of bridge transit limitations is more evident when the detoured traffic flow is forced to bypass a short restricted highway segment, which is numerically captured comparing the functionality levels with 'close' versus 'far' re-entry link, i.e. $\bar{\lambda} = 0.25$ versus $\bar{\lambda} = 0.75$.

Depending on the damage state s_b experienced by the bridge, traffic limitations are applied to the highway networks, leading to a loss of network functionality. This loss can be recovered by the post-event repair actions on the bridge, consequently leading to gradual removal of the traffic limitations. The shape parameters ω and ψ of the bridge recovery profile are selected based on the damage state to be restored. Figure 10 shows the normalised bridge recovery model r_b versus normalised time variable τ with the selected shape parameters for each possible initial damage state. Given the seismic damage and selecting the recovery strategy to restore it, stepwise partial increments of the network functionality at time instants $t_{p,b}$ (where $p = 1, \ldots, s_b$) are obtained when the bridge seismic capacity reaches the target levels r_p up to $\Delta t_{r,b}$, i.e. the final recovery time interval. The shape parameters of the recovery profiles for each initial damage state s_b are listed in Table 6. The corresponding recovery time intervals (adapted from Zhou, Banerjee, & Shinozuka, 2010) and capacity targets (Capacci, 2015) are listed in Table 7.

Figure 11 shows the recovery model for each initial damage state s_b in terms of normalised bridge capacity r_b, stepwise evolution in time of the decision variable d_b and stepwise functionality profiles Q for each studied network by assuming zero idle time and horizon time $t_h = 365$ days. Furthermore, the bar chart in Figure 12 collects the resilience levels R_s of each network given the bridge damage state s_b. These results indicate that, as expected, resilience decreases as the severity of the damage state increases and they allow quantifying the beneficial effects of detours and re-entry links. In particular, network N1 exhibits low levels of resilience with respect to other networks since its recovery profile shows only one jump in functionality related to the complete re-opening of the carriageway to all the users. On the other hand, the bypass associated with the re-entry link close to the restricted highway segment provides to network N3 with $\bar{\lambda} = 0.25$ the largest resilience levels compared to the other networks given the bridge damage state s_b.

Figure 13 shows the intensity-based resilience measure associated with the hazard capacity vector $\boldsymbol{\eta}_i$ for both types of bridge piers. As expected, resilience decreases as the seismic demand increases regardless of the network layout.

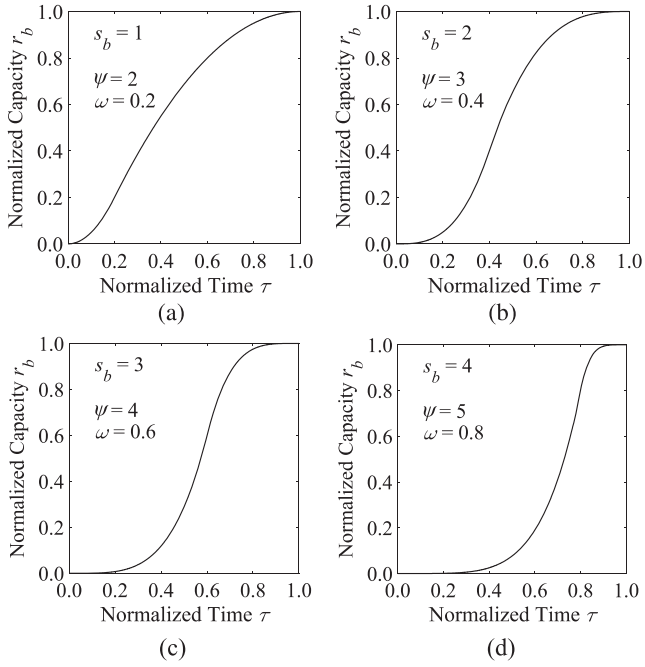

Figure 10. Recovery model of the normalised bridge capacity r_b versus normalised recovery time $\tau = (t - t_i)/(t_r - t_i)$: (a) slight damage, (b) moderate damage, (c) extensive damage, and (d) structural collapse.

Table 6. Shape parameters of the recovery profile for each damage state.

Damage	ω	ψ
SD	0.20	2.0
MD	0.40	3.0
ED	0.60	4.0
SC	0.80	5.0

Table 7. Capacity targets and recovery time intervals for each damage state.

Damage	$r_{p=1}$	$r_{p=2}$	$r_{p=3}$	$r_{p=4}$	$\Delta t_{r,b}$ [days]
SD	1.00	–	–	–	30
MD	0.50	1.00	–	–	90
ED	0.20	0.50	1.00	–	180
SC	0.05	0.20	0.50	1.00	360

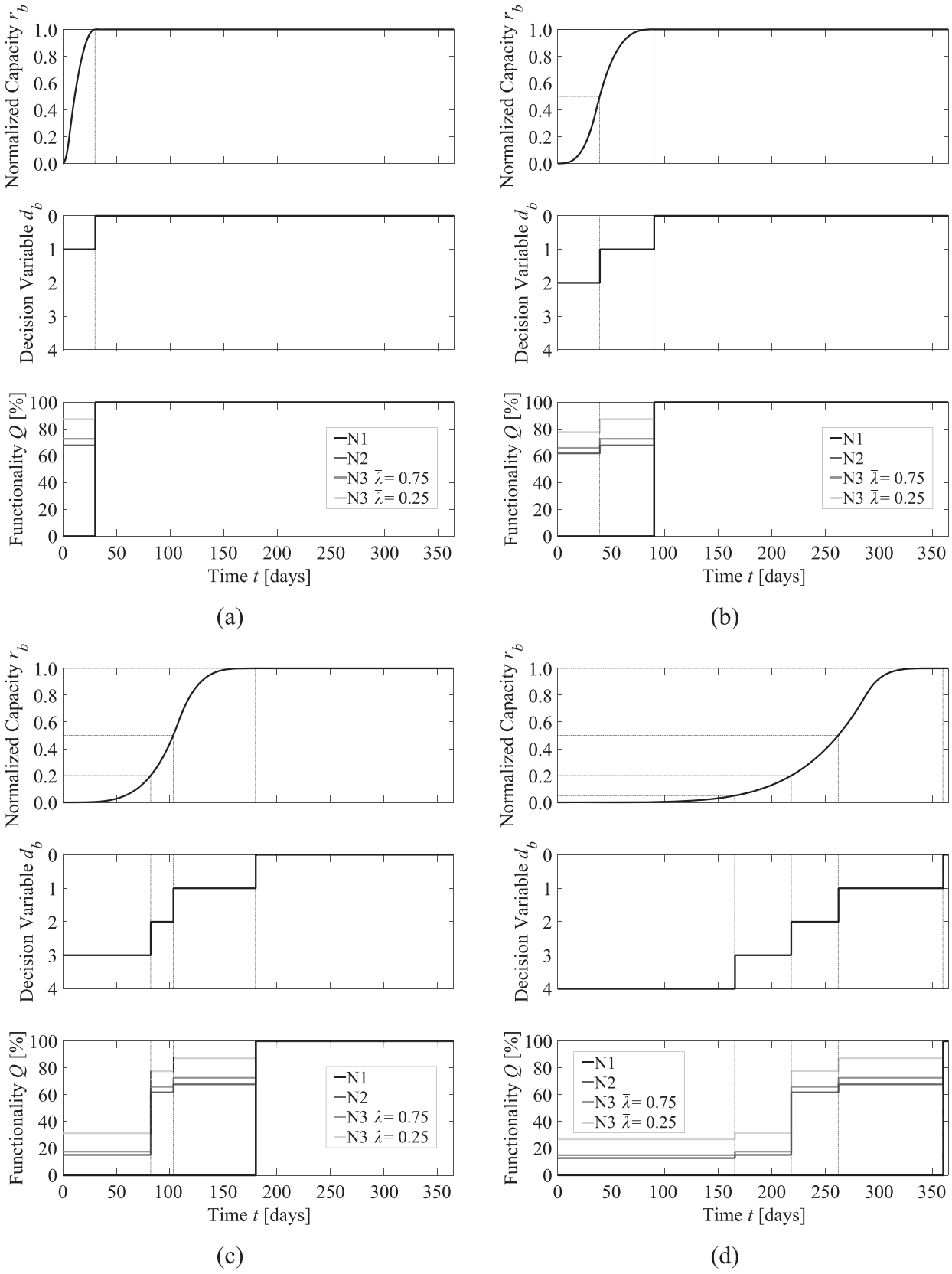

Figure 11. Bridge normalised capacity recovery, bridge decision variable, and network functionality profiles: (a) slight damage, (b) moderate damage, (c) extensive damage, and (d) structural collapse.

The comparison of the results for each road system confirms that detours in combination with re-entry links make the road network more resilient by enhancing the network topological redundancy. Moreover, it is worth mentioning that the remarkably lower vulnerability of the bridge piers with circular cross-section to moderate and extensive

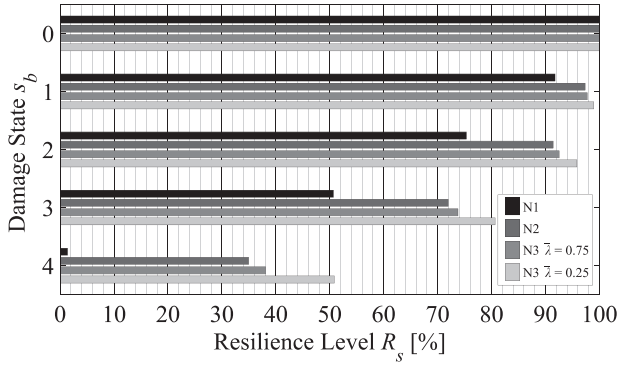

Figure 12. Bar chart of the resilience levels R_s given the bridge damage s_b and the recovery profiles for the networks N1, N2, and N3 with $\bar{\lambda} = 0.25$ and 0.75.

damage states leads to higher values of resilience for seismic events with PGA ranging from about 0.40 g to about 0.80 g.

Effect of aging on the lifetime resilience of highway networks

The deterioration of structural performance due to aging leads to a reduction of seismic resilience during the service life of the road networks. The detrimental effects of structural deterioration on seismic resilience are shown in Figure 14 for network N3 with different re-entry link locations $\bar{\lambda} = 0.25$ and 0.75 and different times of occurrence of the seismic event associated with bridge ages $t_b = 0$, 30 and 60 years. Similar qualitative results can be obtained for the other networks. It is found that resilience is not affected over time up to a limited seismic intensity of about 0.20 g due to the low impact of vulnerability to damage state $s_b = 1$.

Nevertheless, resilience decreases over time by increasing the seismic intensity and, consequently, the probability that the bridge suffers severe damage. Finally, the benefit of a favourable location of the re-entry link on the overall functionality still holds when taking into account structural aging. However, regardless of the network layout and for decreasing values of seismic intensity, the relevant and progressive decay of bridge seismic capacity over time leads resilience to approach the minimum level associated with the bridge collapse.

Resilience of road networks with spatially distributed bridges

Real road networks include multiple bridges and their location within the network may become significantly important depending on the considered earthquake scenario. The two simple road networks shown in Figure 15 are considered to investigate the influence of spatially distributed bridges on lifetime network resilience. The network S consists of a main highway with two identical bridges in series (Figure 15(a)). The network P includes two identical parallel highways with a single bridge along each road segment (Figure 15(b)). Both networks include one origin and one destination and a secondary road to detour the traffic flow. The identical bridges B_1 and B_2 are built at time $t_{c,b} = 0$. With reference to a Cartesian coordinate system $\mathbf{x} = (x,y)$ with origin $\mathbf{x}_c = (0,0)$ in the bridge network centroid and x-axis aligned with the O-D nodes, the coordinates of the bridges are (km): $\mathbf{x}_{b=1} = (-5,0)$ and $\mathbf{x}_{b=2} = (5,0)$ for system S; $\mathbf{x}_{b=1} = (0,-5)$ and $\mathbf{x}_{b=2} = (0,5)$ for system P. The length of the road segments is equal to $L = 15$, 18 and 60 km for the main highway of network S, the two main highways of network P and the detour of both networks, respectively. The other traffic parameters are the same as the ones collected in Table 5. Indeed, the two networks have similar total travel times in unrestricted conditions.

For a highway network with two bridges (i.e. $N_b = 2$) and five possible initial damage states s_b with the related structural recovery profiles (i.e. $N_{s,b} = 5$), the possible initial damage state combinations are $N_s = 5^2 = 25$. Similarly, given the five possible traffic restrictions per bridge d_b, the possible traffic restriction combinations are $N_d = 25$. The bar charts shown in Figure 16 provide the functionality levels for each network restriction combination d. Since redundancy of network S is provided only by the detour, the network functionality is mainly affected by the bridge subjected to the most severe traffic restriction (Figure 16(a)), e.g. the functionality level Q_d with $d_{b=1} = 2$ and $d_{b=2} = 0$ is almost equal to Q_d with $d_{b=1} = 2$ and $d_{b=2} = 1$. Conversely, the network P has a greater topological redundancy and its traffic capacity is significantly harmed only if both bridges are extensively damaged (Figure 16(b)), e.g. the functionality level Q_d with $d_{b=1} = 2$ and $d_{b=2} = 0$ is remarkably larger than Q_d with $d_{b=1} = 2$ and $d_{b=2} = 1$. Analogous comparisons can be drawn for the resilience levels R_s presented for each network damage combination s in

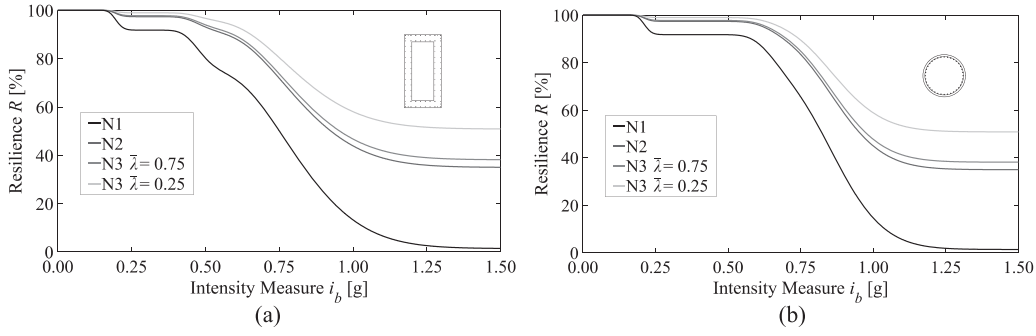

Figure 13. Resilience of networks N1, N2, and N3 with $\bar{\lambda} = 0.25$ and 0.75: bridge piers with (a) hollow-core rectangular cross-section and (b) circular cross-section.

the bar charts in Figure 17, which are defined based on zero idle time, horizon time $t_h = 365$ days, and recovery model defined by the parameters listed in Tables 6 and 7.

The seismic demand is evaluated by the GMPE proposed by Bindi et al. (2011) based on the strong motion database for Italy:

$$\log_{10} i_b = 3.672 + F_D(d_{e,b}, M) + F_M(M) + F_S + F_{sof} \quad (27)$$

$$F_D = [-1.940 + 0.413(M - M_{ref})]\log_{10}\frac{\sqrt{d_{e,b}^2 + h_e^2}}{d_{ref}} - 0.000134\left(\sqrt{d_{e,b}^2 + h_e^2} - d_{ref}\right) \quad (28)$$

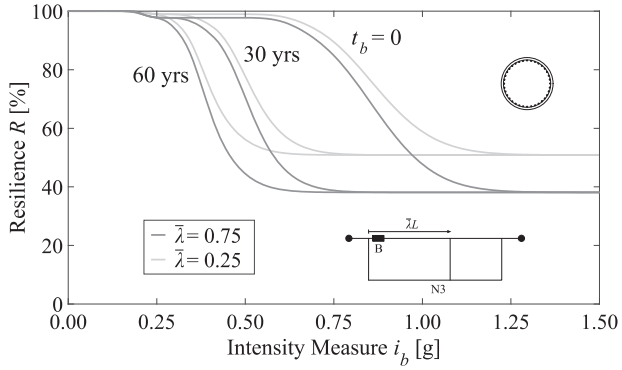

Figure 14. Time-variant resilience of the network N3 with $\bar{\lambda} = 0.25$ and 0.75 for RC bridge piers with circular cross-section and bridge age $t_b = 0$, 30 and 60 years.

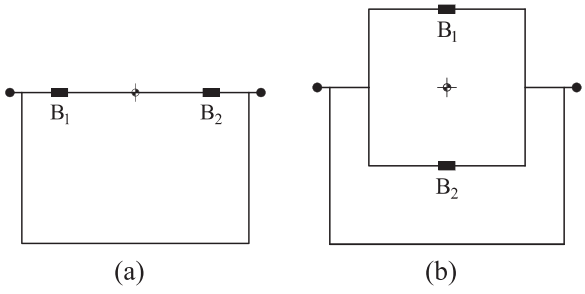

Figure 15. Road networks with two bridges: (a) network S with bridges in series; (b) network P with bridges in parallel.

$$F_M = \begin{cases} -0.626(M - M_{ref}) - 0.0707(M - M_h)^2 & \text{for } M \le M_h \\ 0 & \text{otherwise} \end{cases} \quad (29)$$

where i_b is given in cm/s^2, M is the moment magnitude, $d_{e,b} = ||\mathbf{x}_b - \mathbf{x}_e||$ is the source-to-site distance (in km), $F_D(d_{e,b},M)$, $F_M(M)$, F_S, and F_{sof} are the distance function, the magnitude scaling, the site amplification factor, and the style-of-faulting correction, respectively, $h_e = 10.322$ km is a pseudo-depth parameter, $d_{ref} = 1$ km, $M_{ref} = 5$, and $M_h = 6.75$. Reverse faulting is assumed, with site amplification $F_S = 0.162$ and style-of-faulting correction $F_{sof} = 0.105$.

For a given earthquake magnitude, the bridges are exposed to different seismic demands depending on the epicentre distances. The influence of the earthquake scenario is investigated by considering a square grid of epicentre locations with grid size of 0.2 km, providing the geographical distribution of pointwise resilience measures based on the hazard capacity vector $\boldsymbol{\eta}_e$. Assuming a moment magnitude $M = 6.50$, Figure 18 shows the 3-D surfaces and the contour maps of resilience for network S evaluating the occurrence of a seismic event at specific time during the service life of the structures, namely $t_0 = 50$ years. Two levels of correlation of the bridge seismic capacities are considered: (a) statistical independency and (b) perfect linear correlation.

As expected, resilience decreases as the epicentre approaches the location of the bridges. Due to the limited system redundancy, the most critical earthquake scenarios for both levels of correlation are associated with epicentre locations close to one of the two bridges. However, the impact of the lack of redundancy is partially mitigated increasing the bridge capacity correlation when the epicentre is close to the bridge network centroid $\mathbf{x}_c$. In fact, the likelihood of having at least one bridge severely damaged increases as correlation decreases. Conversely, the most critical earthquake scenarios for the network P are associated with epicentre locations close to $\mathbf{x}_c$, as shown in Figure 19.

This tendency is exacerbated by the correlation of bridge seismic capacities, since for these scenarios the likelihood of having both bridges severely damaged increases with the correlation level. These outcomes emphasise the key role of the mutual influence between earthquake scenario,

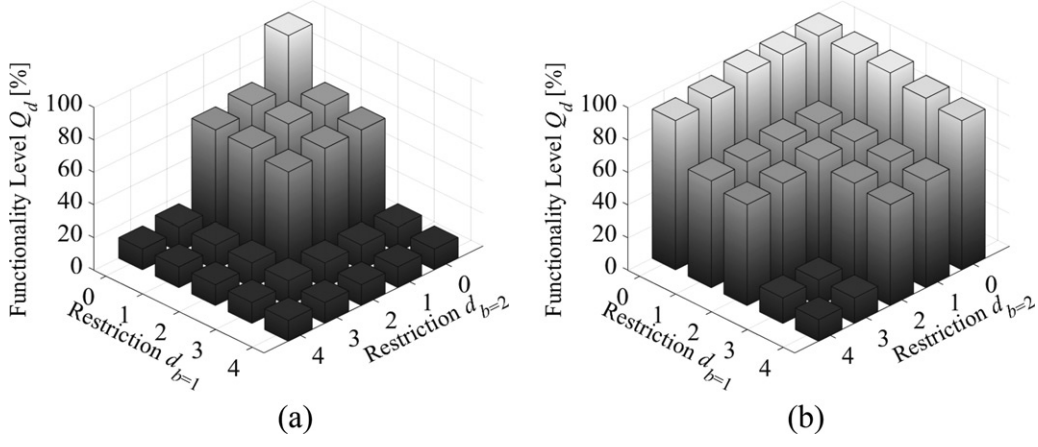

Figure 16. Bar charts of the functionality levels Q_d given the bridge damage combination d: (a) network S; (b) network P.

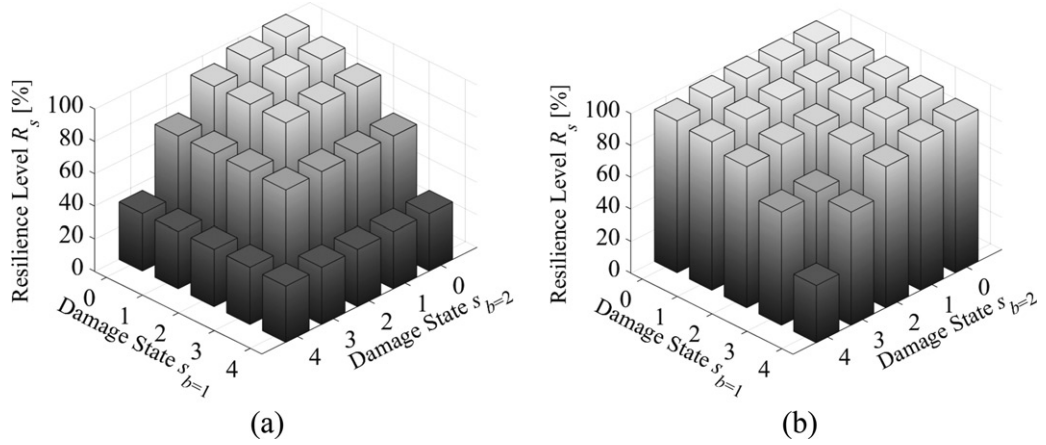

Figure 17. Bar chart of the resilience levels R_s given the bridge damage combination s and the bridge recovery profiles (Figure 8): (a) network S; (b) network P.

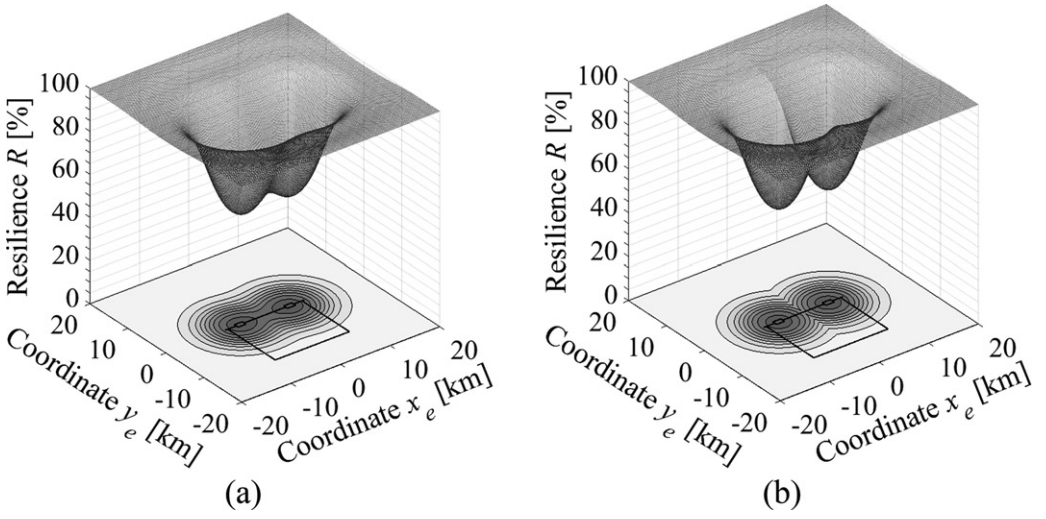

Figure 18. Resilience surfaces and contour maps of network S versus the epicentre location $\mathbf{x}_e = (x_e, y_e)$ for earthquake magnitude $M = 6.50$ and bridge age $t_b = 50$ years: (a) statistically independent and (b) perfectly correlated seismic capacities.

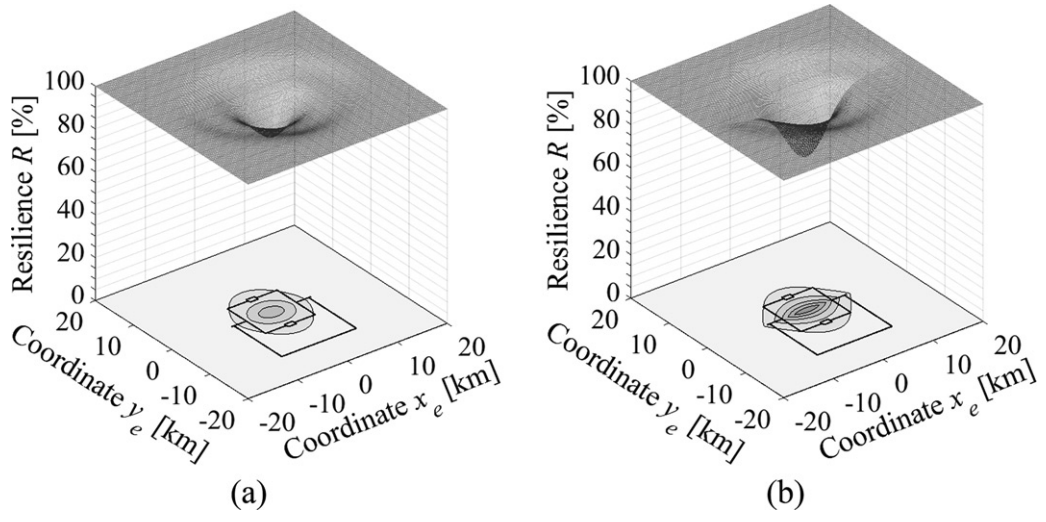

Figure 19. Resilience surfaces and contour maps of network P versus the epicentre location $\mathbf{x}_e = (x_e, y_e)$ for earthquake magnitude $M = 6.50$ and bridge age $t_b = 50$ years: (a) statistically independent and (b) perfectly correlated seismic capacities.

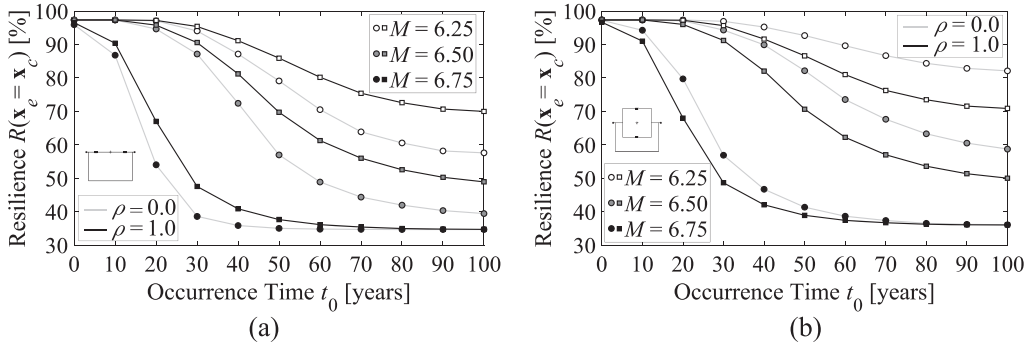

Figure 20. Network resilience R versus the occurrence time t_0 for epicentre location at the bridge network centroid $\mathbf{x}_c$ and earthquake magnitudes $M = 6.25$, 6.50, 6.75: (a) network S; (b) network P.

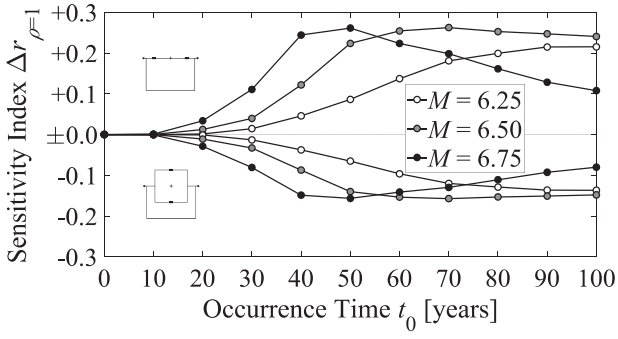

Figure 21. Sensitivity index Δr_ρ of resilience R with epicentre location at the bridge network centroid $\mathbf{x}_c$ for $\rho = 1.0$ versus the occurrence time t_0 for earthquake magnitude $M = 6.25$, 6.50, 6.75.

geographic location of vulnerable structures and system management interventions in a multi-hazard life-cycle-oriented approach to seismic design of resilient structures and infrastructure systems.

Resilience tends to decrease over time due to the detrimental effects of structural deterioration. The impact of the environmental exposure depends on the earthquake scenario and, consequently, on the seismic exposure of the most critical bridges in the network. Figure 20 presents the seismic resilience versus the time of occurrence of the seismic event every 10 years over a 100-year lifetime under different earthquake magnitudes $M = 6.25$, 6.50, and 6.75, and epicentre located at the bridge network centroid, i.e., $\mathbf{x}_e = \mathbf{x}_c$. The progressive decay of resilience depends on the earthquake magnitude based on the considered GMPE. A magnitude $M = 6.75$ induces significantly large probability of simultaneous collapse of both bridges and resilience approaches the corresponding minimum value. For earthquake occurrence from the initial time $t_0 = 0$ to $t_0 = 30$ years the decay rate is significant only for magnitude $M > 6.75$. After significant propagation of corrosion damage, the network resilience is progressively impaired also for the lower magnitudes $M = 6.25$ and 6.50. Nonetheless, the predicted intensity measures on both bridges are such that the probability of severe damage occurrence never reaches large values even at an advanced stage of deterioration.

The aforementioned beneficial effect of bridge capacity correlation for network S, as well as the detrimental effect for network P, can be qualitatively appreciated in Figure 20 by comparing the dashed line with circle markers (i.e. statistically independent case) with the continuous line with square markers (i.e. perfectly correlated case). In order to assess the role of correlation based on a quantitative metric, the following time-variant resilience sensitivity index is introduced:

$$\Delta r_\rho = \frac{R_\rho - R_{\rho=0}}{R_{\rho=0}} \tag{30}$$

where R_ρ is the network seismic resilience associated with a linear correlation coefficient ρ.

Figure 21 illustrates the resilience sensitivity index Δr_ρ for $\rho = 1$, i.e. $\Delta r_{\rho=1}$, in terms of the pointwise resilience measure evaluated in the network centroid $\mathbf{x}_c$ versus the occurrence time t_0 and different magnitudes $M = 6.25$, 6.50 and 6.75. These results confirm the opposite trends obtained for the series system S, with $\Delta r_{\rho=1} > 0$, and the parallel system P, with $\Delta r_{\rho=1} < 0$. Moreover, in both cases the correlation effects tend to increase at the beginning of the service life, after about 10 years, when corrosion damage propagates. However, this tendency is reversed over time under severe deterioration for increasing seismic hazard since both bridges are likely to suffer extensive seismic damage regardless of the level of correlation of their seismic capacities.

Finally, Figure 22 displays the area-based resilience measure R_A associated with the hazard capacity vector $\boldsymbol{\eta}_A$. This synthetic indicator allows assessing the interaction between aging and earthquake scenario on the overall studied region by averaging the pointwise resilience measure along a prescribed area source A_s. In the present application, the area-based resilience measure R_A is computed over a 10-km radius circular area centred in the bridge network centroid $\mathbf{x}_c$. The results confirms the qualitative trends obtained by means of the pointwise measure of resilience in Figure 20.

Nonetheless, the impact of correlation is largely reduced, as also confirmed in Figure 23 by the trend of resilience sensitivity index $\Delta r_{\rho=1}$ in terms of the area-based resilience measure R_A associated with the hazard capacity vector $\boldsymbol{\eta}_A$. The comprehensive representation of the system resilience by means of the proposed average resilience measure R_A allows a direct comparison of the effectiveness of different network management strategies. Thus, the distributed information presented in the contour maps is merged in single parameters, which can properly assist the decision making process. Nevertheless, the indicator R_A depends on the dimension of

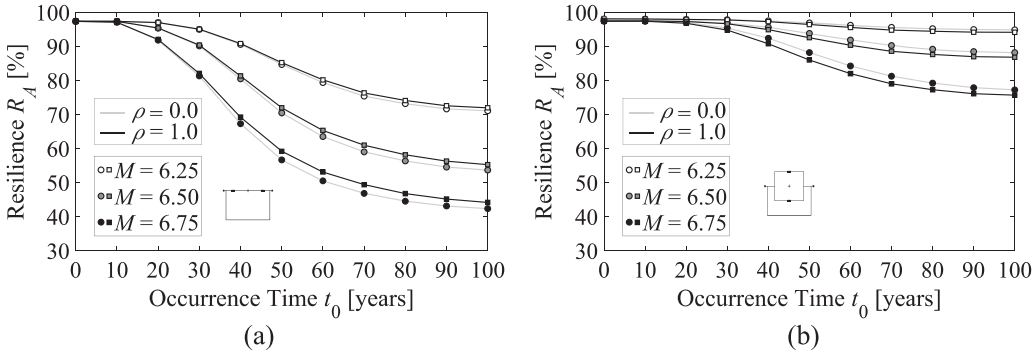

Figure 22. Network resilience R_A, computed over a circular area source with 10-km radius and centre at the bridge network centroid $\mathbf{x}_c$ versus the occurrence time t_0 for earthquake magnitudes $M = 6.25, 6.50, 6.75$: (a) network S; (b) network P.

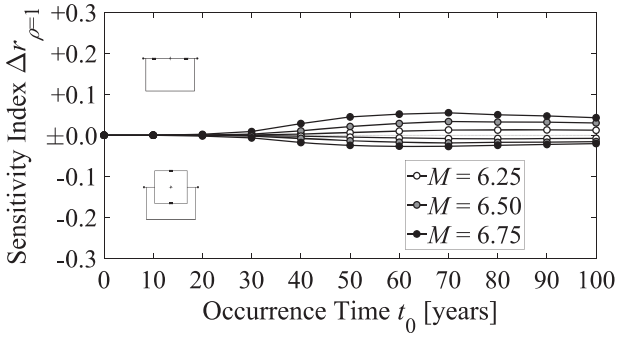

Figure 23. Sensitivity index Δr_ρ of the resilience R_A over a circular area source with 10-km radius and centre at the bridge network centroid $\mathbf{x}_c$ for $\rho = 1.0$ versus the occurrence time t_0 for earthquake magnitude $M = 6.25, 6.50, 6.75$.

the seismic area source and on the likelihood of occurrence of a seismic event with given magnitude in a specific epicentre within the estimated area source. For example, an increase in the size of the area source leads to a reduction of the average resilience decay rate because larger areas enclose epicentre locations too far from the bridges to induce relevant probability of large damage (Capacci & Biondini, 2018c).

Conclusions

A multi-hazard probabilistic framework for life-cycle seismic resilience assessment of road transportation networks has been presented in this article considering spatially distributed RC bridges exposed to chloride-induced corrosion and different earthquake scenarios. Simple road networks have been investigated to demonstrate the capability of the proposed framework to qualitatively and quantitatively assess the interdependency between seismic hazard scenario and environmental exposure of spatially distributed vulnerable bridges in the affected region by means of a set of congestion-based resilience measures that comprehensively assess the time-variant performance of the transportation infrastructure.

The results highlighted that, as expected, detours in combination with re-entry links allow reducing the loss of functionality and, consequently, make the transportation lifeline more resilient with respect to seismic events. However, it has been found that environmental aggressiveness can significantly reduce over time the seismic capacity of bridges and exacerbate in this way the impact on infrastructure resilience of large functionality drops and late restoration processes. In addition, the decay in time of seismic resilience due to aging processes can remarkably depend on the seismic exposure in terms of earthquake magnitude, source-to-site distance and geographical features of the seismic source.

The presented applicative examples are simple compared with complex real case transportation infrastructure systems. Nevertheless, they incorporate some of the most relevant features of the investigated research problem. It has been shown that for networks with bridges in series, which rely on detour routes to ensure a certain degree of redundancy, the most critical earthquake scenarios are associated with epicentres close to the bridges. The impact of the lack of redundancy can be partially mitigated by correlation between bridge seismic capacities when the epicentre is relatively far from the bridges.

In fact, in this case the likelihood of having at least one bridge severely damaged tends to increase as correlation decreases. Conversely, for parallel bridge networks the most critical earthquake scenarios are associated with epicentres close to the bridge network centroid. This is emphasised by bridge capacity correlation, since in these scenarios the likelihood of having severely damaged bridges increases with correlation. Moreover, for the investigated series and parallel networks the correlation effects tend to increase under moderate levels of structural deterioration. However, over time the combined exposure to severe corrosion and seismic damage may significantly reduce such effects.

The resilience framework presented herein can assist decision makers in the definition of effective, reliable, and sustainable emergency management strategies informed by life-cycle multi-hazard probabilistic criteria. To this purpose, future studies should investigate the interaction between traffic restrictions and residual bridge seismic capacities, as well as between direct repair costs and socioeconomic consequences induced by downtime and lack of network connectivity for complex real case transportation infrastructure systems.

Further research is needed also for a more complete understanding of the processes involved in the earthquake-induced disruptions of road networks and communities and their effective and prompt recovery by prioritising the interventions on individual bridges. This includes the role of

several features of the recovery process, including idle time, recovery time, target functionality, horizon time, and recovery profiles with time-variant parameters related to type, severity, and location of seismic damage. The proposed framework may also be adapted to take into account more in-depth knowledge on the mutual interaction of different earthquake-related hazards of spatially distributed vulnerable structures, such as landslides, site amplification effects, liquefaction, and cumulative damage induced by multiple mainshocks or mainshock-aftershock sequences, among others.

Disclosure statement

No potential conflict of interest was reported by the authors.

ORCID

Luca Capacci http://orcid.org/0000-0002-1450-1987
Fabio Biondini http://orcid.org/0000-0003-1142-6261

References

Al-Harthy, A. S., Stewart, M. G., & Mullard, J. (2011). Concrete cover cracking caused by steel reinforcement corrosion. *Magazine of Concrete Research*, *63*(9), 655–667. doi:10.1680/macr.2011.63.9.655

Almusallam, A. A. (2001). Effect of degree of corrosion on the properties of reinforcing steel bars. *Construction and Building Materials*, *15*(8), 361–368. doi:10.1016/S0950-0618(01)00009-5

Ang, A. H. S., & Tang, W. H. (1984). *Probability concepts in engineering planning and design. Volume II: Decision, risk, and reliability*. Hoboken, NJ: Wiley.

Ang, A. H. S., & Tang, W. H. (2007). *Probability concepts in engineering: Emphasis on applications to civil and environmental engineering* (Vol. I, 2nd ed.), Hoboken, NJ: Wiley.

Apostolopoulos, C. A., & Papadakis, V. G. (2008). Consequences of steel corrosion on the ductility properties of reinforcement bar. *Construction and Building Materials*, *22*(12), 2316–2324. doi:10.1016/j.conbuildmat.2007.10.006

American Society of Civil Engineers (ASCE). (2017). *Report card for America's infrastructure*. Reston, VA: ASCE.

Basöz, N., & Kiremidjian, A. S. (1998). *Evaluation of bridge damage data from the Loma Prieta and Northridge*, California earthquakes. Technical Report, MCEER-98-0004.

Baker J.W., 2009. An introduction to probabilistic seismic hazard analysis (PSHA). White Paper, version 1.3.

Bertolini, L., Elsener, B., Pedeferri, P., & Polder, R. (2004). *Corrosion of steel in concrete*. Weinheim, Germany: Wiley-VCH.

Billah, M. A. H. M., & Alam, S. M. (2015). Seismic fragility assessment of highway bridges: a state-of-the-art review. *Structure and Infrastructure Engineering*, *11*(6), 804–832.

Bindi, D., Pacor, F., Luzi, L., Puglia, R., Massa, M., Ameri, G., & Paolucci, R. (2011). Ground motion prediction equations derived from the Italian strong motion database. *Bulletin of Earthquake Engineering*, *9*(6), 1899–1920. doi:10.1007/s10518-011-9313-z

Biondini, F., Bontempi, F., Frangopol, D. M., & Malerba, P. G. (2004). Cellular automata approach to durability analysis of concrete structures in aggressive environments. *Journal of Structural Engineering*, *130*(11), 1724–1737. doi:10.1061/(ASCE)0733-9445(2004)130:11(1724)

Biondini, F., Bontempi, F., Frangopol, D. M., & Malerba, P. G. (2006). Probabilistic service life assessment and maintenance planning of concrete structures. *Journal of Structural Engineering*, *132*(5), 810–825. doi:10.1061/(ASCE)0733-9445(2006)132:5(810)

Biondini, F., Camnasio, E., & Palermo, A. (2014). Lifetime seismic performance of concrete bridges exposed to corrosion. *Structure and Infrastructure Engineering*, *10*(7), 880–900. doi:10.1080/15732479.2012.761248

Biondini, F., Camnasio, E., & Titi, A. (2015a). Seismic resilience of concrete structures under corrosion. *Earthquake Engineering & Structural Dynamics*, *44*(14), 2445–2466. doi:10.1002/eqe.2591

Biondini, F., Capacci, L., & Titi, A. (2015b). Seismic resilience of bridges and highway networks. In *16th Congress of the Italian Association of Earthquake Engineering (ANIDIS 2015)*, L'Aquila, Italy, September 13–17.

Biondini, F., Capacci, L., & Titi, A. (2017). Life-cycle resilience of deteriorating bridge networks under earthquake scenarios. In *16th World Conference on Earthquake Engineering* (16WCEE), Santiago, Chile, January 9–13.

Biondini, F., & Frangopol, D. M. (2016). Life-cycle performance of deteriorating structural systems under uncertainty: Review. *Journal of Structural Engineering*, *142*(9), F4016001–F4016017. doi:10.1061/(ASCE)ST.1943-541X.0001544

Biondini, F., & Frangopol, D. M. (2018). Life-cycle performance of civil structure and infrastructure systems: Survey. *Journal of Structural Engineering*, *144*(1), 06017007–06017008. doi:10.1061/(ASCE)ST.1943-541X.0001923

Biondini, F., & Vergani, M. (2015). Deteriorating beam finite element for nonlinear analysis of concrete structures under corrosion. *Structure and Infrastructure Engineering*, *11*(4), 519–532. doi:10.1080/15732479.2014.951863

Bocchini, P., & Frangopol, D. M. (2011). A stochastic computational framework for the joint transportation network fragility analysis and traffic flow distribution under extreme events. *Probabilistic Engineering Mechanics*, *26*(2), 182–193. doi:10.1016/j.probengmech.2010.11.007

Bocchini, P., Decò, A., & Frangopol, D. M. (2012). Probabilistic functionality recovery model for resilience analysis. In *6th International Conference on Bridge Maintenance, Safety and Management (IABMAS 2012)*, Stresa, Italy, July 8–12 (*Bridge Maintenance, Safety, Management, Resilience and Sustainability*, F. Biondini and D. M. Frangopol (Eds.), CRC Press/Balkema, Taylor & Francis Group, London, UK, 2012).

Bocchini, P., & Frangopol, D. M. (2012a). Optimal resilience- and cost-based post-disaster intervention prioritization for bridges along a highway segment. *Journal of Bridge Engineering*, *17*(1), 117–129. doi:10.1061/(ASCE)BE.1943-5592.0000201

Bocchini, P., & Frangopol, D. M. (2012b). Restoration of bridge networks after an earthquake: multicriteria intervention optimization. *Earthquake Spectra*, *28*(2), 426–455. doi:10.1193/1.4000019

Bruneau, M., Chang, S. E., Eguchi, R. T., Lee, G. C., O'Rourke, T. D., Reinhorn, A. M., Shinozuka, M., Tierney, K., Wallace, W. A., & Winterfeldt, D. V. (2003). A framework to quantitatively assess and enhance the seismic resilience of communities. *Earthquake Spectra*, *19*(4), 733–752. doi:10.1193/1.1623497

Bruneau, M., & Reinhorn, A. M. (2007). Exploring the concept of seismic resilience for acute care facilities. *Earthquake Spectra*, *23*(1), 41–62. doi:10.1193/1.2431396

Burton, H. V., Deierlein, G., Lallemant, D., & Lin, T. (2015). Framework for incorporating probabilistic building performance in the assessment of community seismic resilience. *Journal of Structural Engineering*, *142*(8), C4015007. doi:10.1061/(ASCE)ST.1943-541X.0001321

Cabrera, J. G. (1996). Deterioration of concrete due to reinforcement steel corrosion. *Cement and Concrete Composites*, *18*(1), 47–59. doi:10.1016/0958-9465(95)00043-7

Capacci, L. (2015). *Seismic resilience of bridge networks* (Master thesis). Politecnico di Milano, Milan, Italy.

Capacci, L., Biondini, F., & Titi, A. (2016). Seismic resilience of aging bridges and transportation networks. In: 8th International Conference on Bridge Maintenance, Safety and Management (IABMAS 2016), Foz do Iguaçu, Brazil, June 26–30 (*Maintenance, Monitoring, Safety, Risk and Resilience of Bridges*, T. Bittencourt, D.M. Frangopol and A. Beck (Eds.), CRC Press/Balkema, Taylor & Francis Group, London, UK).

Capacci, L., & Biondini, F. (2018a). Effects of structural deterioration and infrastructure upgrading on the life-cycle seismic resilience of bridge networks. In *IABSE Conference "Engineering the Developing World"*, Kuala Lumpur, Malaysia, April 25–27.

Capacci, L., & Biondini, F. (2018b). Life-cycle seismic resilience of aging bridges and road networks considering bridge capacity correlation. In 9th International Conference on Bridge Maintenance, Safety and Management, July 9–13, Melbourne, Australia (*Maintenance, Safety, Risk, Management and Life-cycle Performance of Bridges*, N. Powers, D.M. Frangopol, R. Al-Mahaidi and C. Caprani (Eds.), CRC Press/Balkema, Taylor & Francis Group, London, UK).

Capacci, L., & Biondini, F. (2018c). Role of the earthquake scenario on life-cycle seismic resilience of aging bridge networks. In *16th European Conference on Earthquake Engineering*, Thessaloniki, Greece, June 18–21.

Carturan, F., Pellegrino, C., Rossi, R., Gastaldi, M., & Modena, C. (2013). An integrated procedure for management of bridge networks in seismic areas. *Bulletin of Earthquake Engineering*, *11*(2), 543–559. doi:10.1007/s10518-012-9391-6

CEN-EN 1998-1. (2004). Eurocode 8: Design of structures for earthquake resistance – Part 1: General rules, seismic actions and rules for buildings. European Committee for Standardization, Brussels.

Chang, S. E., & Shinozuka, M. (2004). Measuring improvements in the disaster resilience of communities. *Earthquake Spectra*, *20*(3), 739–755. doi:10.1193/1.1775796

Chang, S. E. (2009). Infrastructure resilience to disasters. *Frontiers of Engineering, National Academy of Engineering*, *39*(4), 36–41.

Cimellaro, G. P., Reinhorn, A. M., & Bruneau, M. (2010a). Framework for analytical quantification of disaster resilience. *Engineering Structures*, *32*(11), 3639–3649. doi:10.1016/j.engstruct.2010.08.008

Cimellaro, G. P., Reinhorn, A. M., & Bruneau, M. (2010b). Seismic resilience of a hospital system. *Structure and Infrastructure Engineering*, *6*(1–2), 127–144. doi:10.1080/15732470802663847

Cornell, C. A. (1968). Engineering seismic risk analysis. *Bulletin of the Seismological Society of America*, *58*(5), 1583–1606.

Decò, A., Bocchini, P., & Frangopol, D. M. (2013). A probabilistic approach for the prediction of seismic resilience of bridges. *Earthquake Engineering & Structural Dynamics*, *42*(10), 1469–1487. doi:10.1002/eqe.2282

Der Kiureghian, A., & Song, J. (2008). Multi-scale reliability analysis and updating of complex systems by use of linear programming. *Reliability Engineering & System Safety*, *93*(2), 288–297. doi:10.1016/j.ress.2006.10.022

Dolšek, M. (2009). Incremental dynamic analysis with consideration of modeling uncertainties. *Earthquake Engineering and Structural Dynamics*, *38*(6), 805–825.

Elnashai, A. S., & Di Sarno, L. (2008). *Fundamentals of earthquake engineering*. Hoboken, NJ: Wiley.

Erath, A., Birdsall, J., Axhausen, K. W., & Hajdin, R. (2009). Vulnerability assessment methodology for Swiss road network. *Transportation Research Record: Journal of the Transportation Research Board*, *2137*(1), 118–126. TRB, Washington, DC, USA. doi:10.3141/2137-13

Evans, S. P. (1976). Derivation and analysis of some models for combining trip distribution and assignment. *Transportation Research*, *10*(1), 37–57. doi:10.1016/0041-1647(76)90100-3

fib. (2006). *Model Code for service life design*. Bulletin 34, Fédération internationale du béton/International Federation for Structural Concrete.

Franchin, P., & Cavalieri, F. (2015). Probabilistic assessment of civil infrastructure resilience to earthquakes. *Computer-Aided Civil and Infrastructure Engineering*, *30*(7), 583–600. doi:10.1111/mice.12092

Frank, M., & Wolfe, P. (1956). An algorithm for quadratic programming. *Naval Research Logistics Quarterly*, *3*(1–2), 95–110. doi:10.1002/nav.3800030109

Frangopol, D. M. (2011). Life-cycle performance, management, and optimisation of structural systems under uncertainty: accomplishments and challenges. *Structure and Infrastructure Engineering*, *7*(6), 389–413. doi:10.1080/15732471003594427

Ghosh, J., Rokneddin, K., Padgett, J. E., & Dueñas-Osorio, L. (2014). Seismic reliability assessment of aging highway bridge networks with field instrumentation data and correlated failures, I: Methodology. *Earthquake Spectra*, *30*(2), 795–817. doi:10.1193/040512EQS155M

Gilbert, S. W. (2010). *Disaster resilience: A guide to the literature. NIST Special Publication 1117*. National Institute of Standards and Technology, Office of Applied Economics Building and Fire Research Laboratory, Gaithersburg, MD.

Glicksman, M. E. (2000). *Diffusion in solids*. New York, NY: Wiley.

Guzmán, S., Gálvez, J. C., & Sancho, J. M. (2011). Cover cracking of reinforced concrete due to rebar corrosion induced by chloride penetration. *Cement and Concrete Research*, *41*(8), 893–902. doi:10.1016/j.cemconres.2011.04.008

Iman, R. L., & Conover, W. J. (1982). A distribution-free approach to inducing rank correlation among input variables. *Communications in Statistics—Simulation and Computation*, *11*(3), 311–334. doi:10.1080/03610918208812265

Isaković, T., & Fischinger, M. (2000). Regularity indices for bridge structures. In *12th World. Conference on Earthquake Engineering (12WCEE)*, Auckland, New Zealand, January 30–February 4.

Iwasaki, T., Fujino, Y., Iemura, H., Ikeda, S., Kemada, H., Katayama, T., Kawashima, K., Onishi, Y., Saeki, S., & Toki, K. (1995). *Report on highway bridge damage caused by the Hyogo-ken Nanbu Earthquake of 1995*. Committee on Highway Bridge Damage, Japan.

Jia, G., & Gardoni, P. (2018). State-dependent stochastic models: A general stochastic framework for modeling deteriorating engineering systems considering multiple deterioration processes and their interactions. *Structural Safety*, *72*, 99–110. doi:10.1016/j.strusafe.2018.01.001

Kang, W. H., Song, J., & Gardoni, P. (2008). Matrix-based system reliability method and applications to bridge networks. *Reliability Engineering & System Safety*, *93*(11), 1584–1593. doi:10.1016/j.ress.2008.02.011

Kafali, C., & Grigoriu, M. (2005). Rehabilitation decision analysis. In 9th International Conference on Structural Safety and Reliability (ICOSSAR'05), Rome, Italy, June 19–23 (*Safety and Reliability of Engineering Systems and Structures*, G. Augusti, G. Schuëller and M. Ciampoli (Eds.), Millpress, 2773–2780).

Karamlou, A., & Bocchini, P. (2017a). From component damage to system-level probabilistic restoration functions for a damaged bridge. *Journal of Infrastructure Systems*, *23*(3), 04016042. doi:10.1061/(ASCE)IS.1943-555X.0000342

Karamlou, A., & Bocchini, P. (2017b). Functionality-fragility surfaces. *Earthquake Engineering & Structural Dynamics*, *46*(10), 1687–1709. doi:10.1002/eqe.2878

Kumar, R., & Gardoni, P. (2014). Renewal theory-based life-cycle analysis of deteriorating engineering systems. *Structural Safety*, *50*, 94–102. doi:10.1016/j.strusafe.2014.03.012

Mackie, K. R., & Stojadinović, B. (2006). Post-earthquake functionality of highway overpass bridges. *Earthquake Engineering & Structural Dynamics*, *35*(1), 77–93. doi:10.1002/eqe.534

Mander, J., Priestley, M., & Park, R. (1988). Theoretical stress-strain model for confined concrete. *Journal of Structural Engineering*, *114*(8), 1804–1826. doi:10.1061/(ASCE)0733-9445(1988)114:8(1804)

Mander, J. B., Dhakal, R. P., Mashiko, N., & Solberg, K. M. (2007). Incremental dynamic analysis applied to seismic financial risk assessment of bridges. *Engineering Structures*, *29*(10), 2662–2672. doi:10.1016/j.engstruct.2006.12.015

Martin, W. A., & McGuckin, N. A. (1998). *Travel estimation techniques for urban planning*. National Cooperative Highway Research Program (NCHRP), Report 365, National Academy Press, Washington, DC.

Mazzoni, S., McKenna, F., Scott, M. H., Fenves, G. L., et al. (2006). *OpenSees: open system for earthquake engineering simulation. OpenSees command language manual*. Berkeley, CA: Pacific Earthquake Engineering Research Center, University of California.

Ni, P., Petrini, L., & Paolucci, R. (2014). Direct displacement-based assessment with nonlinear soil-structure interaction for multi-span reinforced concrete bridges. *Structure and Infrastructure Engineering*, *10*(9), 1211–1227. doi:10.1080/15732479.2013.802813

Padgett, J. E., & DesRoches, R. (2007). Bridge functionality relationships for improved seismic risk assessment of transportation networks. *Earthquake Spectra*, *23*(1), 115–130. doi:10.1193/1.2431209

Papageorgiou, G., Mouratidis, A., & Eliou, N. (2012). Comprehensive model for upgrading two-lane road network. *European Transport Research Review*, *4*(3), 125–135. doi:10.1007/s12544-012-0071-z

Paulay, T., & Priestley, M. J. N. (1992). *Seismic design of reinforced concrete and masonry structures*. Hoboken, NJ: Wiley.

Pinto, A. V., Verzeletti, G., Magonette, G., Pegon, P., Negro, P., & Guedes, J. (1996). Pseudo-dynamic testing of large-scale R/C bridges in ELSA. In *11th World Conference on Earthquake Engineering* (11WCEE), Acapulco, Mexico, June 23–28.

Priestley, M. J. N., Calvi, G. M., & Kowalsky, M. J. (2007). *Displacement-based seismic design of structures*. Pavia, Italy: IUSS Press.

Sharma, N., Tabandeh, A., & Gardoni, P. (2018). Resilience analysis: A mathematical formulation to model resilience of engineering systems. *Sustainable and Resilient Infrastructure*, *3*(2), 49–67. doi:10.1080/23789689.2017.1345257

SIMQKE. (1976). *A program for artificial ground motion generation. User's Manual and Documentation*. Cambridge, MA: NISEE, Department of Civil Engineering, Massachusetts Institute of Technology. doi:10.19070/2167-8685-SI04001

Sanchez-Silva, M., Klutke, G. A., & Rosowsky, D. V. (2011). Life-cycle performance of structures subject to multiple deterioration mechanisms. *Structural Safety*, *33*(3), 206–217. doi:10.1016/j.strusafe.2011.03.003

Structural Engineers Association of California (SEAOC). (1995). *Vision 2000: Performance-based seismic engineering of buildings*. Sacramento, CA: SEAOC.

Song, J., & Ok, S. Y. (2010). Multi-scale system reliability analysis of lifeline networks under earthquake hazards. *Earthquake Engineering & Structural Dynamics*, *39*(3), 259–279.

Takeda, T., Sozen, M. A., & Nielsen, N. N. (1970). Reinforced concrete response to simulated earthquake. *Journal of the Structural Division*, *11*(2), 10–21.

Thomson, R. C., & Richardson, D. E. (1995). A graph theory approach to road network generalisation. In *17th International Cartographic Conference (ICC 1995)*, Barcelona, Spain, September 3–9.

Titi, A., & Biondini, F. (2013). Resilience of concrete frame structures under corrosion. In 11th International Conference on Structural, Safety & Reliability (ICOSSAR 2013), New York, NY, June 16–20 (*Safety, reliability, risk and life-cycle performance of structures and infrastructures*, G. Deodatis, B. R. Ellingwood and D. M. Frangopol (Eds.), CRC Press/Balkema, Taylor & Francis Group, London, UK).

Titi, A., & Biondini, F. (2016). On the accuracy of diffusion models for life-cycle assessment of concrete structures. *Structure and Infrastructure Engineering*, *12*(9), 1202–1215. doi:10.1080/15732479.2015.1099110

Titi, A., Biondini, F., & Frangopol, D. M. (2015). Seismic resilience of deteriorating concrete structures. In: N. Ingraffea and M. Libby (Eds.), Structures Congress 2015, Portland, OR, April 23–25. ASCE.

Vamvatsikos, D., & Cornell, C. A. (2002). Incremental dynamic analysis. *Earthquake Engineering & Structural Dynamics*, *31*(3), 491–514. doi:10.1002/eqe.141

Venkittaraman, A., & Banerjee, S. (2014). Enhancing resilience of highway bridges through seismic retrofit. *Earthquake Engineering & Structural Dynamics*, *43*(8), 1173–1191. doi:10.1002/eqe.2392

Vidal, T., Castel, A., & Francois, R. (2004). Analyzing crack width to predict corrosion in reinforced concrete. *Cement and Concrete Research*, *34*(1), 165–174. doi:10.1016/S0008-8846(03)00246-1

Vořechovský, M., & Novák, D. (2009). Correlation control in small-sample Monte Carlo type simulations I: A simulated annealing approach. *Probabilistic Engineering Mechanics*, *24*(3), 452–462. doi:10.1016/j.probengmech.2009.01.004

Wardrop, J. G. (1952). Some theoretical aspects of road traffic research. *Proceedings of the Institution of Civil Engineers*, *1*(3), 325–362. doi:10.1680/ipeds.1952.11259

Yang, D. Y., & Frangopol, D. M. (2019). Life-cycle management of deteriorating civil infrastructure considering resilience to lifetime hazards: A general approach based on renewal-reward processes. *Reliability Engineering & System Safety*, *183*, 197–212. doi:10.1016/j.ress.2018.11.016

Yashinsky, M. (1995). Damage to bridges and highways from the Northridge earthquake. The Northridge, California, Earthquake, *116*, 163–185.

Zanini, M. A., Faleschini, F., & Pellegrino, C. (2017). Probabilistic seismic risk forecasting of aging bridge networks. *Engineering Structures*, *136*, 219–232. (doi:10.1016/j.engstruct.2017.01.029

Zhang, R., Castel, A., & François, R. (2010). Concrete cover cracking with reinforcement corrosion of RC beams during chloride-induced corrosion process. *Cement and Concrete Research*, *40*(3), 415–425. doi:10.1016/j.cemconres.2009.09.026

Zhou, Y., Banerjee, S., & Shinozuka, M. (2010). Socio-economic effect of seismic retrofit of bridges for highway transportation networks: a pilot study. *Structure and Infrastructure Engineering*, *6*(1–2), 145–157. doi:10.1080/15732470802663862